remote sensing

MDPI

Article

Performance of the CMORPH and GPM IMERG Products over the United Arab Emirates

Tareefa S. Alsumaiti [1], Khalid Hussein [1,2,*], Dawit T. Ghebreyesus [3] and Hatim O. Sharif [3]

[1] Geography and Urban Sustainability Department, College of Humanities and Social Sciences, United Arab Emirates University, Al-Ain P.O. Box 15551, UAE; tareefa@uaeu.ac.ae

[2] Cooperative Institute for Research in Environmental Sciences (CIRES), University of Colorado, Boulder, CO 80309, USA

[3] Department of Civil and Environmental Engineering, University of Texas and San Antonio, San Antonio, TX 78249, USA; dawit.ghebreyesus@my.utsa.edu (D.T.G.); hatim.sharif@utsa.edu (H.O.S.)

* Correspondence: khalid.hussein@uaeu.ac.ae

Received: 18 March 2020; Accepted: 29 April 2020; Published: 1 May 2020

Abstract: Satellite-based precipitation products are becoming available at very high temporal and spatial resolutions, which has accelerated their use in various hydro-meteorological and hydro-climatological applications. Because the quantitative accuracy of such products is affected by numerous factors related to atmospheric and terrain properties, validating them over different regions and environments is needed. This study investigated the performance of two high-resolution global satellite-based precipitation products: the climate prediction center MORPHing technique (CMORPH) and the latest version of the Integrated Multi-SatellitE Retrievals for the Global Precipitation Mission (GPM) algorithm (IMERG), V06, over the United Arab Emirates from 2010 through 2018. The estimates of the products and that of 71 in situ rain gauges distributed across the country were compared by employing several common quantitative, categorical, and graphical statistical measures at daily, event-duration, and annual temporal scales, and at the station and study area spatial scales. Both products perform quite well in rainfall detection (above 70%), but report rainfall not observed by the rain gauges at an alarming rate (more than 30%), especially for light rain (lower quartile). However, for moderate and intense (upper quartiles) rainfall rates, performance is much better. Because both products are highly correlated with rain gauge observations (mostly above 0.7), the satellite rainfall estimates can probably be significantly improved by removing the bias. Overall, the CMORPH and IMERG estimates demonstrate great potential for filling spatial gaps in rainfall observations, in addition to improving the temporal resolution. However, further improvement is required, regarding the overestimation and underestimation of small and large rainfall amounts, respectively.

Keywords: United Arab Emirates; precipitation; CMORPH; GPM

1. Introduction

As a vital component of the hydrologic cycle, precipitation is characterized by its chaotic nature, the short time scale over which it can occur and evolve, and high variability in the temporal and spatial domains [1,2]. Precipitation rates and accumulations can be measured directly at the ground level by using sensors, for instance, rain gauges and disdrometers, or such information can be inferred from measurements of remote sensing instruments such as ground-based and airborne radar, as well as microwave and infrared (IR) sensors aboard satellites [3,4]. Rainfall measurements by remote sensors provide large areal coverage and are available at high spatial and temporal resolutions; however, their accuracy is limited because of different sources of systematic and random errors. Atmospheric conditions, terrain characteristics, electromagnetic repertoire of the rainfall particles, the sensor type, and spatial and temporal resolutions can all lead to such errors [2,5].

High-resolution precipitation data (temporal and spatial) have been examined in many recent studies [6–12]. Ground-based weather radars estimate precipitation at very high spatial and temporal resolutions, with real-time monitoring over a large area (relative to rain gauges) [13,14]. However, radar measurements can be influenced by the terrain, and radar networks are not available in most developing countries, due to cost and lack of technical expertise [5,15]. Unlike weather radars, satellite-based precipitation products provide the means for timely near-global precipitation estimates. The latest satellite-based precipitation products measure precipitation with very high spatial and temporal resolutions [4]. To achieve these resolutions, they combine IR images with passive microwave echoes to produce precipitation estimates. Realizing the huge potential of satellite-based precipitation products, researchers across the world have conducted significant studies to verify and validate them [5,16–24]. However, their performance must be further verified, particularly in arid and semi-arid regions and regions with complex terrain [23].

The enhancement of the spatial and temporal resolutions of multi-satellite sensor precipitation measurements is leading to improved performance when compared with that of ground-based measurements [23,25–27]. The National Aeronautics and Space Administration (NASA) Tropical Rainfall Measuring Mission (TRMM) Multi-Satellite Precipitation Analysis (TMPA) has been providing high quality precipitation estimates for about two decades [26]. Several state-of-the art products were based on TRMM data, including different versions of TRMM 3B42 and the Artificial Neural Networks—Climate Data Record (PERSIANN) products [27]. Another global product is the gauge-adjusted Global Satellite Mapping of Precipitation (GSMaP) produced at the Earth Observation Research Center (EORC) of the Japan Exploration Agency (JAXA) [28]. Two of the most commonly used multi-satellite sensor precipitation products are the Climate Prediction Center MORPHing technique (CMORPH) and the Integrated Multi-SatellitE Retrievals (IMERG) for the Global Precipitation Mission (GPM).

The CMORPH uses morphing techniques to compute precipitation estimates derived from microwave observations integrated with the information obtained from geostationary satellite IR data [29]. With an 8-km resolution at the equator, the CMORPH has a slight advantage in spatial resolution over other products and covers the 1998–present period, thus encompassing the entire combined period of the GPM and the Tropical Rainfall Measuring Mission (TRMM). The GPM provides global precipitation estimates in nearly real time, however, occasionally, there are data stream interruptions. The mission is composed of more than 10 satellites and the GPM Core Observatory satellite, which was commissioned by NASA and JAXA. The main goal of the mission is to improve previous precipitation products by increasing the visit time and enhancing the precipitation algorithms [30]. The GPM provides users with various levels of products, ranging from raw data to precipitation rates. Deployed in 2014, it provides IMERG rainfall products at a spatial resolution of $0.1^\circ \times 0.1^\circ$ and a temporal resolution of 30 min. The final IMERG product (Level 3) is designed to incorporate, merge, and inter-calibrate all precipitation microwave estimates along with IR satellite estimates, ground precipitation gauges, and all other precipitation estimators involved in the era of the TRMM satellites [31].

The majority of validation and verification studies have shown that the performance of the recent satellite rainfall products varies spatially and is dependent on the hydro-climatic characteristics of the region [32,33]. For example, Shen et al. [34] found that the CMORPH performed better in capturing the spatial and temporal patterns of precipitation over China compared with the TRMM 3B42 product and PERSIANN. However, the CMORPH was found to be the least accurate in capturing the spatial pattern of rainfall over Indonesia, as compared with the results of other satellite-based products [35]. Wehbe et al. [23] concluded that an earlier version of the CMORPH (v0.x) failed to produce a significant correlation with rain gauges over the United Arab Emirates (UAE); their findings were in line with the results of a study by Ghajarnia [36] that was conducted over the Urmia Basin in Iran. In contrast, Li et al. [3] reported that the correlation between a rain gauge network and the CMORPH was the highest among other precipitation products (TRMM and PERSIANN) over the Yangtze River in China.

Duan et al. [37] also demonstrated that the CMORPH is among the best performing products over the Adige Basin in Italy.

Satellite-based products, such as IMERG, are usually outperformed by those of ground-based radars. Tang et al. [38] evaluated the latest IMERG product at hourly and daily time scales over China and compared it to nine satellite and reanalysis products and demonstrated that the product improved over time, outperforming CMORPH throughout the study period (2000–2018). A study conducted in southeast China revealed that radar mosaic quantitative precipitation estimates exhibited a higher correlation coefficient than that of the IMERG at the grid level scale [39]. The product exhibited acceptable agreement with the rain gauge data in central and West Africa, except in mountainous regions [40]. Evaluation of different IMERG hourly products over a large river basin in China revealed that their performance was satisfactory at different spatial and temporal scales [41]. Anjum et al. [42] evaluated the performance of IMERG and two TRMM products over the northern high lands of Pakistan. They reported that, while all products correlated well with gauge observations, the IMERG estimates were more reliable for all seasons. Furthermore, they observed that all satellite products overestimated light rainfall and underestimated heavy rainfall. Wang et al. [43] compared IMERG V05B and TRMM to ground-based observations under complex topographic and climatic conditions over the northwest arid region of China. Their results demonstrated that IMERG correlated better with ground-based observations, but had higher bias, especially for light precipitation.

The improvement of IMERG products over time in detecting and quantifying rainfall is widely reported in several studies (e.g., [44–47]). Li et al. [48] examined the uncertainty of five satellite-based precipitation products, ground-based observations, and model reanalysis output over mainland China. They concluded that the overall performance of IMERG was better than the other satellite products, followed by TRMM and CMORPH. Zhang et al. [49] compared the performance of IMERG, TRMM, and CMORPH over the Tianshan Mountains in China. They found that IMERG outperformed TRMM and CMORPH in estimating daily precipitation, especially for light and moderate precipitation events. Lee et al. [50] conducted a study to evaluate TRMM, IMERG, and CMORPH products over East Asia. Their results indicated that satellite products effectively captured daily variations in precipitation from spring to fall, with relatively low correlations in the winter. The verification of daily detection for various rainfall thresholds indicated that IMERG and TRMM products exhibited high correlations with ground observations, while CMORPH showed persistent underestimation for all thresholds, especially in the winter.

Few studies have assessed remotely sensed precipitation data over dry countries like the UAE, where freshwater resources are limited and water security is a top priority often spelled out by officials. For example, Adeyewa and Nakamura [51] compared TRMM rainfall data to gauge observations over five major African climatic regions: arid, semiarid, savanna, tropical wet, and the South Atlantic Ocean. They observed that satellite bias was higher in the dry seasons when rainfall is small and was highest over dryer areas. Dinku et al. [52] evaluated four satellite products over dry regions in East Africa and suggested that the satellite products overestimated rainfall, most of the time due to sub-cloud evaporation. Sultana and Nasrollahi [53] assessed five global high-resolution satellite precipitation products (two PERSIANN products, two TRMM products, and CMORPH) in eastern and western parts of Saudi Arabia, using 29 rain gauges data. The satellite data were evaluated on a daily and monthly scale, and at a $0.25^\circ \times 0.25^\circ$ spatial resolution. Their evaluation revealed that most of the products performed poorly in estimating rainfall during the dry season and somewhat better during the wet season. Overall, CMORPH performed better than the other products over Saudi Arabia.

The main objective of this study is to evaluate the performance of the two main satellite-based precipitation products (CMORPH and IMERG) in comparison with rain gauge observations over the UAE for the 2010–2018 period, to assess their potential in water resources and hydrologic applications in this arid country, that occasionally suffers from extreme rainfall events. Various statistical evaluation metrics are used at different temporal and spatial scales. A brief description of the study area and the rainfall datasets used is provided in Section 2, and the analysis methodology is described in Section 3.

The results are presented and discussed in Section 4, followed by the study summary and conclusions in Section 5.

2. Study Area and Data

2.1. Study Area

The UAE is located on the southeastern tip of the Arabian Peninsula bounded by the Arabian Gulf and the Gulf of Oman (Figure 1). It lies between 22°39′ and 26°04′ north latitude and between 51°30′ and 56°24′ east longitude [54]. The country consists of seven emirates that cover an area of around 83,600 km^2, the majority of which is very dry desert. Neighboring countries include the Kingdom of Saudi Arabia to the south and west and the Sultanate of Oman to the north and east. The climate of the UAE is subtropical–arid, with hot summers and warm winters. Approximately 90% of the land has a climate categorized as a hot desert climate [55], which is characterized by excessive evapotranspiration rates. In the summer, the maximum temperatures reach above 45 °C (113 °F) on the coastal plain. The average maximum temperatures in July and August, as reported by the National Center of Meteorology (NCM), are 38.9 °C and 40.3 °C, respectively [56]. The precipitation in the UAE is very scarce and highly sporadic, both spatially and temporally [55]. The spatial distribution of the average annual precipitation over the country shows that the wettest regions are located in the northeastern part of the country. The mean annual rainfall in the UAE is about 78 mm and ranges from 40 mm in the southern desert region to over 160 mm in the northeastern mountains and adjacent coastal areas [57]. Although recent years witnessed several extreme rainfall events, time series analysis of precipitation in the country shows a breakpoint in 1999, after which precipitation significantly decreased [55].

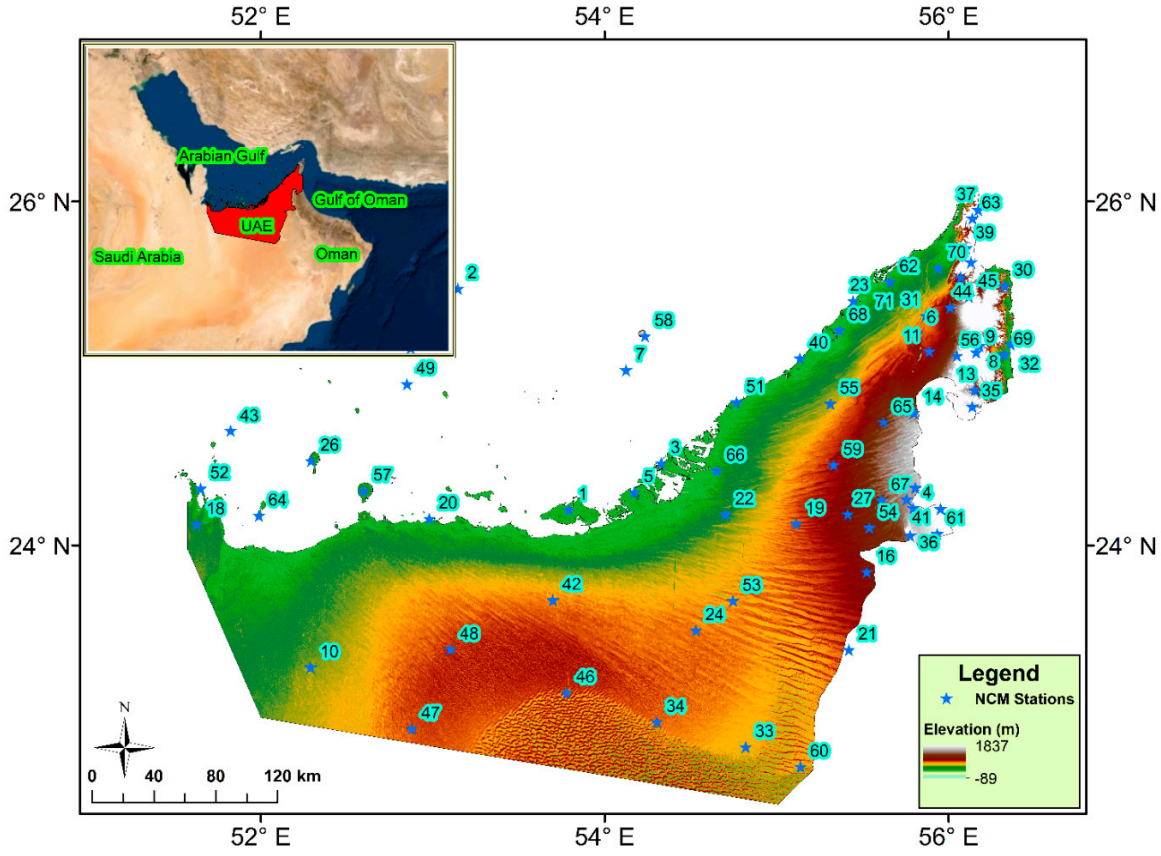

Figure 1. Map of the United Arab Emirates (UAE) and the National Center of Meteorology network of 71 rain gauge stations used in the study.

2.2. Data

The datasets employed in this study include ground-based in situ rainfall measurements and satellite-based rainfall data. The rain gauge data were obtained from the UAE NCM rain gauge network. The spatial distribution of the rain gauge stations over the country can be seen in Figure 1. The timeframe of the analysis spans nine years (2010–2018). Daily rainfall data from 71 NCM rain gauge stations were used in the assessment. The gauges report rainfall measurements electronically with a threshold of 0.2 mm.

CMORPH multi-satellite-based precipitation data were acquired from the official FTP server of the Climate Prediction Center of the National Oceanic and Atmospheric Administration (ftp://ftp.cpc.ncep.noaa.gov/precip/). Two versions of the CMORPH multi-satellite precipitation products are available: (1) CMORPH-V0.x, and (2) CMORPH-V1.0. The main difference between the two is that CMORPH_V1.0 is reprocessed with a fixed algorithm (same algorithm is used throughout the timeframe) and uses inputs of the same version; this is mainly done to reduce the substantial inhomogeneity introduced by the evolving algorithm of the CMORPH_V0.x. The timeframe in the latest version is expanded to cover the period from 1998 to present, whereas the previous version only covered the 2002–2018 period. The Version 1.0 include the raw, satellite only precipitation estimates as well as bias-corrected and gauge-satellite blended precipitation products. The bias-corrected version of CMORPH_V1.0 was employed in this study, and the wet months were used for the analysis with the monthly CMORPH data stored in one compressed (.tar) file format. There are several products in both versions that differ in their temporal and spatial resolutions. The product with an 8 × 8 km spatial resolution and 30-min temporal resolution was selected for this study.

IMERG is one of several GPM products and is available in three product levels: Early, Late, and Final; the first two levels are near real time with a latency time of four and 12 h after observation, respectively. The final run with latency of up to two months after observation requires gauge analysis correlation and produces a product that is expected to have the best accuracy and quality [31]. This study utilized the IMERG Final run with 0.1° × 0.1° spatial resolution and 30 min temporal resolution; it covers the period from June 2000 of the TRMM era up to the current latency, and can be downloaded from http://pmm.nasa.gov/data-access/downloads. The IMERG algorithm inter-calibrates, merges, and interpolates all satellite-based microwave estimates together with microwave-calibrated IR satellite estimates [31]. Version 6 of IMERG (IMERG-V06) is the latest and fourth version of the IMERG algorithm since its inception in 2014. The product includes a variety of new features, such as increasing the maximum rainfall threshold from 50 to 200 mm/h, full inter-calibration to the GPM combined instrument dataset, the use of an updated rain retrieval algorithm, and incorporation of the Advanced Technology Microwave Sounder (ATMS) dataset. Estimates from the Sondeur Atmosphérique du Profil d'Humidité Intertropicale par Radiométrie (SAPHIR) instrument are incorporated into IMERG for the first time in version 6. Moreover, IMERGV06B applies a new time interpolation scheme based on modern-era retrospective reanalysis 2 and Goddard earth observing system model (GEOS) forward processing (FP), for processing data by using total column water vapor instead of IR data [58]. More details about the different GPM products and IMERG algorithms are available in [31,58,59].

3. Methodology

3.1. Data Processing

Significant data processing was needed for satellite products, especially in the case of the CMORPH data, due to the need for reformatting to raster datasets over the study area. The second step was to extract the data of the rain gauge stations from the CMORPH and IMERG raster datasets. The nearest neighbor algorithm was used to extract the data for the stations, by assuming the station data were the same as the closest point from the stations to the raster center. The last step was to aggregate the sub-hourly data to daily data, such that the rain gauge temporal resolution matched. The final output of the data processing was a time series of the rain gauge, CMORPH, and IMERG data for each station.

3.2. Performance Measures

For spatially averaged rainfall, we compared annual rainfall totals, probability density functions (pdfs) of daily rainfall occurrence of the satellite-based products, and rain gauge observations. We also investigated the systematic and random errors of the satellite-based products, by calculating relative mean error (RME) and centralized root mean square error (CRMSE). The systematic errors are related to the sensors and are usually one directional (e.g., under- or over-estimation and can be detected through MRE), while random errors (evident in CRMSE values) depend on the sensor sampling [58].

For detailed quantitative comparison of the satellite-based products versus in situ observations, different types of statistical measures were used [7,54,60,61], which are divided into three groups: (A) the rainfall detection contingency of the products; (B) bias and error measures; and (C) measures of the agreement between the satellite-based products and rain gauges. The rainfall detection contingency measures are very important in determining the ability of the satellite-based product to detect a storm event. The most common measures include the probability of detection (POD), false alarm rate (FAR), and critical success index (CSI). POD can be referred to as the hit rate of the satellite-based product. In contrast, FAR, which is referred to as false positives, quantifies the probability of the satellite to falsely report the occurrence of rainfall that was not observed by the rain gauges. CSI is a more conservative way of calculating the probability of satellite-based product accuracy (more detailed information on POD, FAR, and CSI is available in [62]).The degree of agreement between the satellite-based products and rain gauge observations was quantified by using the Pearson CC. To quantify the error of the satellite-based product, four statistical measures were applied. These include the mean absolute error (MAE) and mean error (ME), which captures the average error without any weight added to the error distribution. The root mean square error (RMSE) was used to obtain the average error by giving higher weight to large errors. The relative bias (RBIAS) was another way to capture error, specifically by representing the spatial distribution of the systematic bias of the satellite-based products. The detailed formulae for all the performance measures are provided in Table 1.

Table 1. List of the statistical indices used for validation of CMORPH and IMERG data [a].

Statistical Index	Units	Equation	Perfect Value
Relative mean error (RME)	Ratio	$RME = \frac{\sum_{i=1}^{n}(S_i - G_i)}{\sum_{i=1}^{n} G_i}$	0
Centralized root mean square error (CRMSE)	Ratio	$CRMSE = \frac{\sqrt{\frac{1}{N}\sum_{i=1}^{n}\left[S_i - G_i - \frac{1}{N}\sum_{i=1}^{n}(S_i - G_i)\right]^2}}{\frac{1}{N}\sum_{i=1}^{n} G_i}$	0
Probability of detection (POD)	Ratio	$POD = \frac{P_{SG}}{P_{SG}+P_G}$	1
False alarm rate (FAR)	Ratio	$FAR = \frac{P_S}{P_{SG}+P_S}$	0
Critical success index (CSI)	Ratio	$CSI = \frac{P_{SG}}{P_{SG}+P_S+P_G}$	1
Pearson correlation coefficient (CC)	Ratio	$CC = \frac{\sum_{i=1}^{n}(G_i - \overline{G})(S_i - \overline{S})}{\sqrt{\sum_{i=1}^{n}(G_i - \overline{G})^2} * \sqrt{\sum_{i=1}^{n}(S_i - \overline{S})^2}}$	1
Mean absolute error (MAE)	mm	$MAE = \frac{1}{n}\sum_{i=1}^{n}\lvert S_i - G_i\rvert$	0
Mean error (ME)	mm	$ME = \frac{1}{n}\sum_{i=1}^{n}(S_i - G_i)$	0
Root mean square error (RMSE)	mm	$RMSE = \sqrt{\frac{1}{n}\sum_{i=1}^{n}(S_i - G_i)^2}$	0
Relative bias (RBIAS)	%	$RBIAS = \frac{\sum_{i=1}^{n}(S_i - G_i)}{\sum_{i=1}^{n} G_i} * 100$	0

[a] N_i is the number of days; n, number of samples; S_i, satellite precipitation estimate; G_i, gauged observation; P_{SG}, observed rain correctly detected; P_G, observed rain not detected; P_S, rain detected but not observed.

4. Results and Discussion

4.1. Evaluation of Spatially Averaged Rainfall

Figure 2A shows the total annual precipitation across the UAE over the studied 9-year period, as estimated by the rain gauge networks and satellite-based products. The spatially averaged annual rainfall ranged between 10.99 mm in 2012 and 179.19 mm in 2013, with an average of 54.17 mm/year. The two satellite-based products followed the annual trends recorded by the rain gauge network. However, IMERG-V06 overestimated the annual rain gauge observations for seven of the nine years, whereas the CMORPH underestimated the annual rainfall for six years.

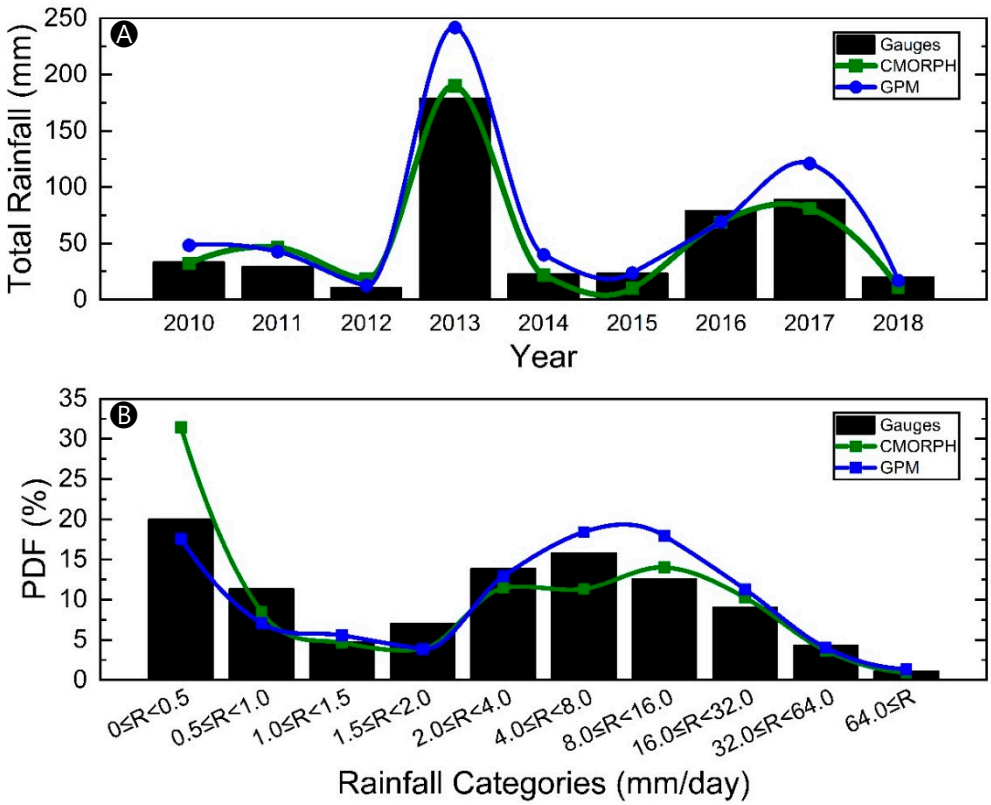

Figure 2. (**A**) The total annual precipitation (averaged over the UAE); (**B**) Probability density functions (pdfs) of daily average rainfall occurrence grouped by intensity interval for rain gauges (bars), Integrated Multi-SatellitE Retrievals (IMERG)-V06 (blue), and Climate Prediction Center MORPHing technique (CMORPH) (green).

The frequency of daily precipitation for different spatially averaged values observed by the rain gauge network is presented in Figure 2B. Rainfall intensities R are shown at intervals of 0–0.5, 0.5–1.0, 1.0–1.5, 1.5–2.0, 2.0–4.0, 4.0–8.0, 8.0–16.0, 16.0–32.0, 32.0–64.0, and >64.0 mm/day. The distribution of daily rain gauge rainfall is bimodal, with peaks at the lowest rainfall (0 = < R < 0.5 mm/day), and moderate rainfall (4 = < R < 8 mm/day). The highest precipitation (R > 32 mm/day) is less frequent in comparison with that of the rest of the intervals. In general, both satellite-based products capture the daily rainfall PDF particularly well. IMERG-V06 performs much better than CMORPH for the lowest daily rainfall, however, it overestimates the number of moderate and high rainfall events.

The RME, a measure of the systematic bias of satellite-based products, is shown in Figure 3A; it was computed for nine quantiles (Q) of spatially averaged daily rainfall R ($R \leq Q20$, $Q20 < R \leq Q40$, $Q40 < R \leq Q60$, $Q60 < R \leq Q80$, $Q80 < R \leq Q85$, $Q85 < R \leq Q99$, $Q90 < R \leq Q95$, $Q95 < R \leq Q99$, and $Q99 < R$). Both satellite-based products overestimate rainfall in the lowest quantiles (positive RME values) and slightly underestimate the rainfall in higher quantiles (small negative

RME values), with RME values dropping significantly from the lowest quantile to the second lowest quantile. The low quantiles represent very light precipitation, where both products significantly overestimate rainfall. The CMORPH performs better when the satellite-based products overestimate rainfall, whereas IMERG-V06 measurements improve slightly (less underestimation) when rainfall is underestimated.

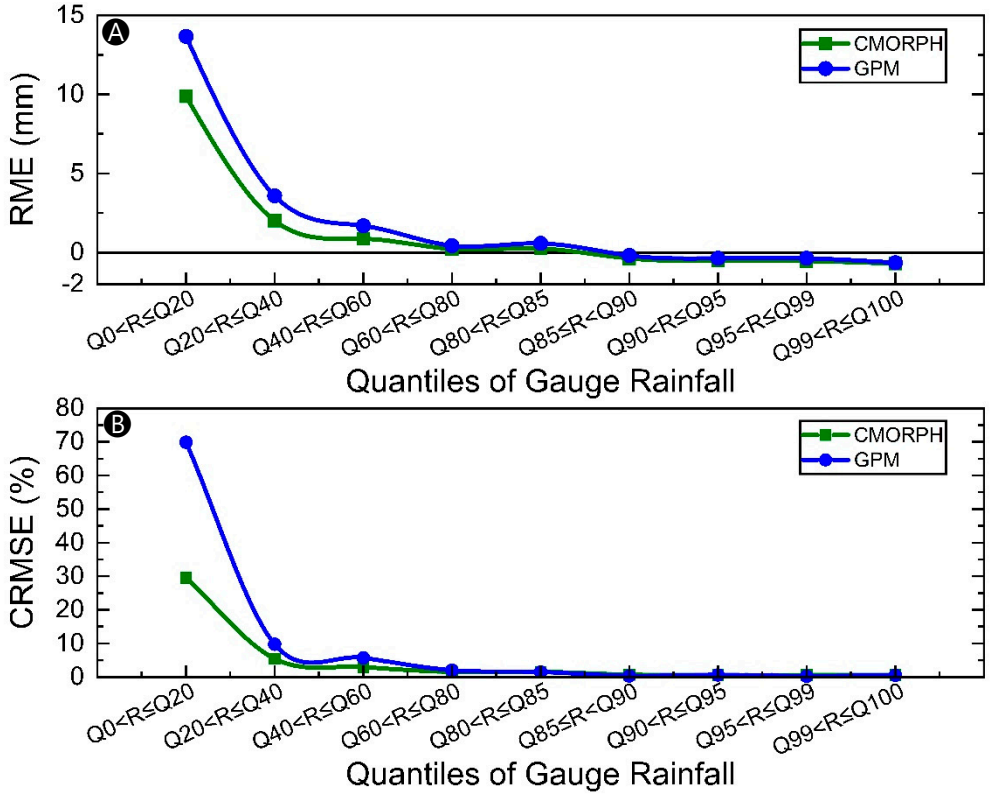

Figure 3. (**A**) Relative mean error (RME) of the IMERG-V06 and CMORPH estimates for different daily rainfall quantiles, based on rain gauge observations; (**B**) Centralized root mean square error (CRMSE) of the IMERG-V06 and CMORPH estimates for different daily rainfall quantiles, based on rain gauge observations.

The random error of the satellite rainfall products for the nine given quantiles is estimated by CRMSE (Figure 3B). Both satellite-based products show high CRMSE values at lower quantile ranges and lower CRMSE values at higher quantile ranges; the CMORPH shows better performance for the lowest four quantiles, and the IMERG-V06 performs better in the other quantiles.

4.2. Station-Based Evaluation

This analysis was conducted by calculating the statistical performance measures over each station separately and then the values of each measure were categorized into five groups to illustrate the spatial patterns.

4.2.1. Rainfall Detection Contingency Measures

The spatial distribution of the POD from both satellite-based products over the stations is quite high for the coastal areas, especially for the northeastern region of the country (Emirates of Dubai, Sharjah, Ras Al Khaimah, and Fujairah) (Figure 4A,D). In general, the POD of the CMORPH is clearly lower than that of the IMERG over the entire country. The average POD across the UAE is 0.83 for IMERG and 0.69 for CMORPH, with median values of about 1.0 and 0.8, respectively. The IMERG resulted in a perfect (1) POD for several stations for most events, whereas the CMORPH had perfect

POD over only four stations. For the IMERG, POD is higher than 0.70 for 83% of the stations, whereas only 58% of the stations have a POD higher than 0.7. The distribution of the POD shows larger variability over the Al Hajar Mountains in the eastern region of the country for the CMORPH.

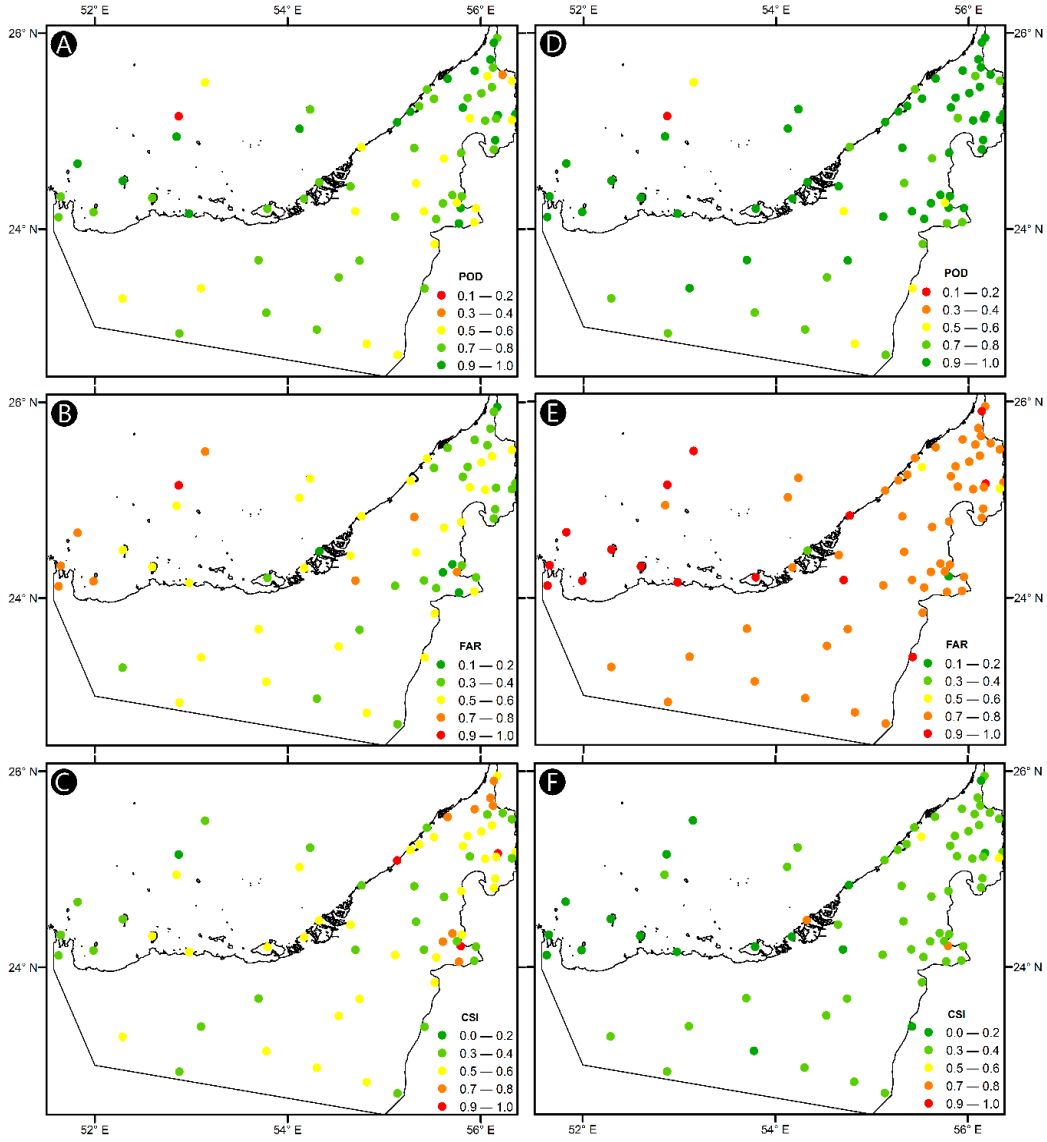

Figure 4. Spatial distribution of the probability of detection (POD) (**A**,**D**), false alarm rate (FAR) (**B**,**E**), and critical success index (CSI) (**C**,**F**) for CMORPH (**A**–**C**) and IMERG—V06 (**D**–**F**) satellite-based products.

Interestingly, the spatial patterns of FAR indicate that the CMORPH far outperforms the IMERG across the entire study area, as shown in Figure 4B,E. In comparison with the IMERG FAR, the CMORPH FAR exhibits significant variability. The high FAR from the IMERG could be attributed to the overestimation of the rainfall from clouds that failed to create measurable rainfall and/or under-catchment by the gauges; i.e. gauge accuracy and sub-cloud evaporation due to aridity of the region and the high temperatures. In addition, the mismatch between point-scale stations and areal satellite products would have a significant effect on evaluation results. For a product to be very accurate and acceptable, it must maintain a balance between the two evaluation parameters (POD and FAR), i.e., exhibiting a high POD while maintaining low FAR. In Figure 4C,F, CSI maps demonstrate that the CMORPH slightly outperforms the IMERG estimate in overall rainfall detection performance.

A summary of the performance measures is provided in Table 2. The details of the performance measures for all rain gauge stations are listed in Appendices A and B.

Table 2. Basic statistics of the performance measures for two satellite rainfall products (CMORPH and IMERG) versus rain gauge measurements.

Group of Performance	Product	Variable	Quartile					Average	Number of Observations
			0%	25%	50%	75%	100%		
Contingency	CMORPH	POD	0.000	0.500	0.800	1.000	1.000	0.692	443
		FAR	0.000	0.000	0.500	0.667	1.000	0.443	443
		CSI	0.000	0.250	0.444	0.592	1.000	0.437	443
	IMERG-V06	POD	0.000	0.885	1.000	1.000	1.000	0.831	464
		FAR	0.000	0.641	0.778	0.875	1.000	0.723	464
		CSI	0.000	0.125	0.222	0.357	1.000	0.270	464
Error and Bias	CMORPH	RMSE (mm)	0.000	0.507	1.884	4.235	42.334	3.106	464
		MAE (mm)	0.000	0.121	0.490	1.297	8.432	0.883	457
		ME (mm)	−7.156	−0.307	0.000	0.374	6.200	0.129	457
		RBIAS (%)	−3.412	−2.227	-0.250	5.732	887.054	8.836	405
	IMERG-V06	RMSE (mm)	0.002	0.824	2.055	4.339	47.689	3.759	457
		MAE (mm)	0.000	0.227	0.652	1.415	15.597	1.214	457
		ME (mm)	−7.900	−0.068	0.121	0.634	15.05	0.498	457
		RBIAS (%)	−3.004	−0.610	2.116	11.805	986.830	19.131	406
Correlation	CMORPH	CC	−0.091	0.505	0.858	0.982	1.000	0.712	395
	IMERG-V06	CC	−0.117	0.497	0.835	0.961	1.000	0.700	406

4.2.2. Bias and Error Measures

The error statistics clearly indicate that both CMORPH and IMERG perform quite well in the southern part of the UAE, as can be seen in Figure 5. The coastal regions show higher error values for both products with the CMORPH having slightly lower error than that of the IMERG. However, the spatial distribution of the RMSE in both products follows similar patterns, especially over the northeastern part of the UAE. Once again, both satellite-based products show higher variability over the Al Hajar Mountains for bias and error measures. About 75% of the stations had an RMSE of <4 mm, with average values of 3.01 and 3.76 mm for the CMORPH and IMERG, respectively. The MAE followed the same spatial pattern of the RMSE for both products, as shown in Figure 7. For the MAE, 60% and 65% of the stations reported an error of <1 mm for the CMORPH and IMERG, respectively (see Appendices A and B). It should be noted that the lowest RMSE for both products is computed in the Al Ain area, with four stations within a few kilometers of each other. The IMERG product demonstrates higher errors over the inland areas than for the coastal areas, especially the northwestern coast. This area is extremely dry with less coverage by rain gauges. Similar to the RMSE results, the CMORPH product slightly outperforms the IMERG in terms of the MAE.

The difference between the products in error and bias measures is illustrated in the ME and RBIAS maps (Figure 6). The IMERG overestimates rainfall over most areas of the country, especially the dry western part. In contrast, the CMORPH underestimates rainfall over most of the southern part of the UAE, with negative average RBIAS. For the CMORPH, the overestimation is limited to some of the coastal and mountainous areas. Stations with acceptable RBIAS (i.e., <10%) exceed 77% of the total stations for the CMORPH and 63% for the IMERG.

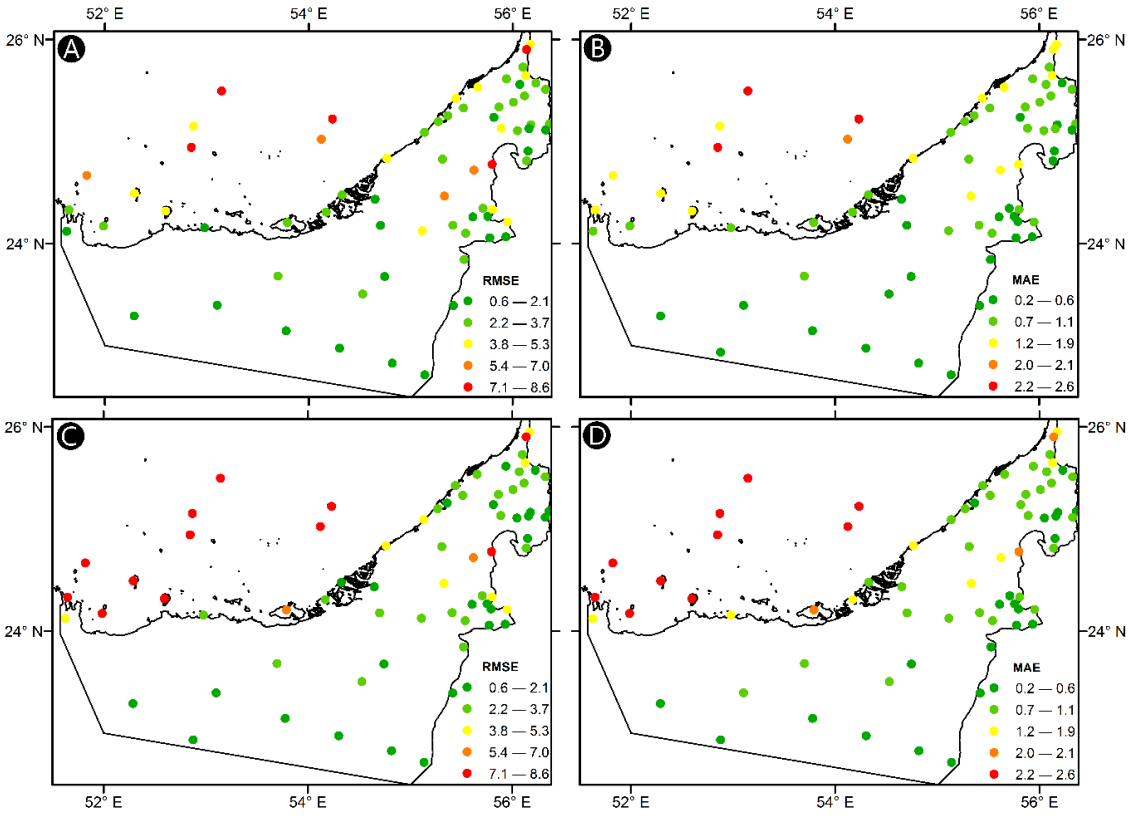

Figure 5. Spatial distribution of root mean square error (RMSE) (**A**,**C**) and mean absolute error (MAE) (**B**,**D**) performance measures for CMORPH (**A**,**B**) and IMERG—V06 (**C**,**D**) products.

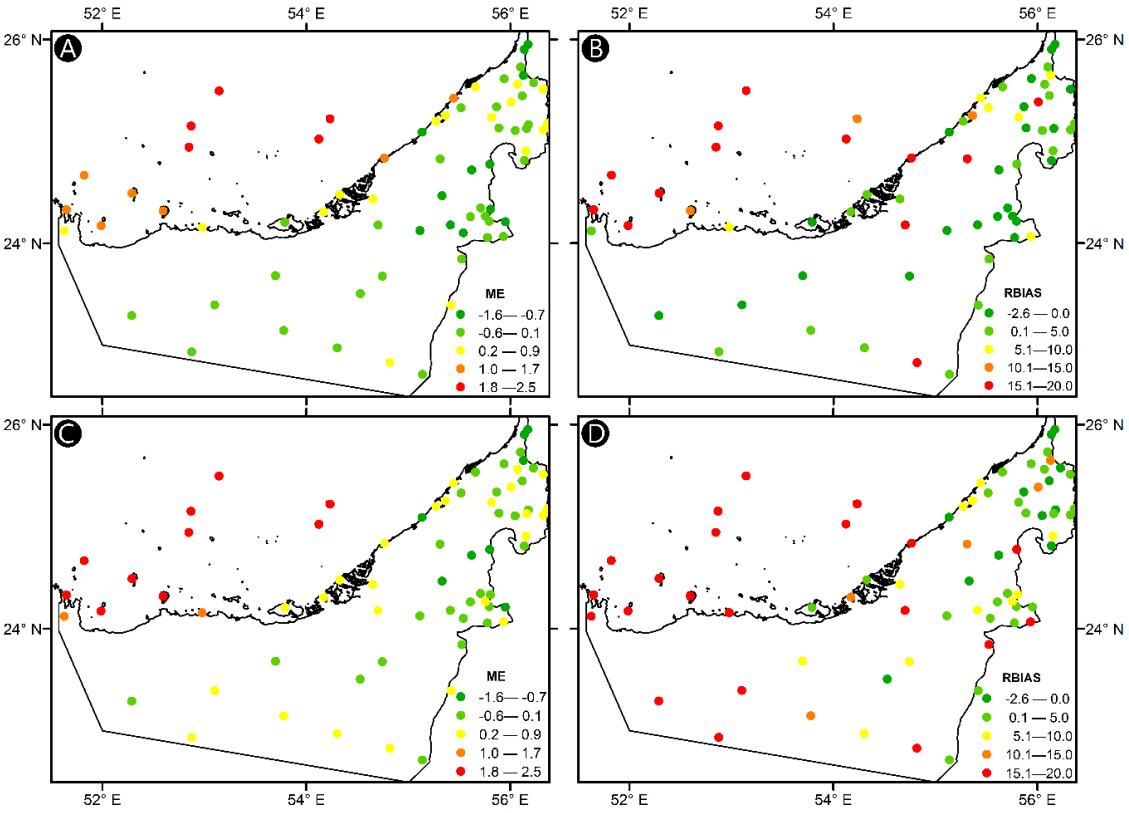

Figure 6. Spatial distribution of mean error (ME) (**A**,**C**) and relative bias (RBIAS) (**B**,**D**) performance measures for CMORPH (**A**,**B**) and IMERG—V06 (**C**,**D**) products.

4.2.3. Rainfall Correlation

The Pearson CC between satellite estimates and rain gauge observations are computed for each station, and then interpolated by using the IDW method. There is a striking similarity in the correlation maps of the two products, as shown in Figure 7. The similarity is not only in their spatial pattern but also in the distribution of the values of the coefficient. The country is generally divided into two parts, with the western part having CCs of <0.6 and the eastern one having >0.6. Both products exhibit an average CC of about 0.7. However, IMERG performs slightly better with a CC higher than 0.8 for 32% of the stations and 27% of the stations for CMORPH. The statistics summary of the CCs are provided in Table 2. The relatively high values of CC are due to the fact that the correlations are computed at daily time scales.

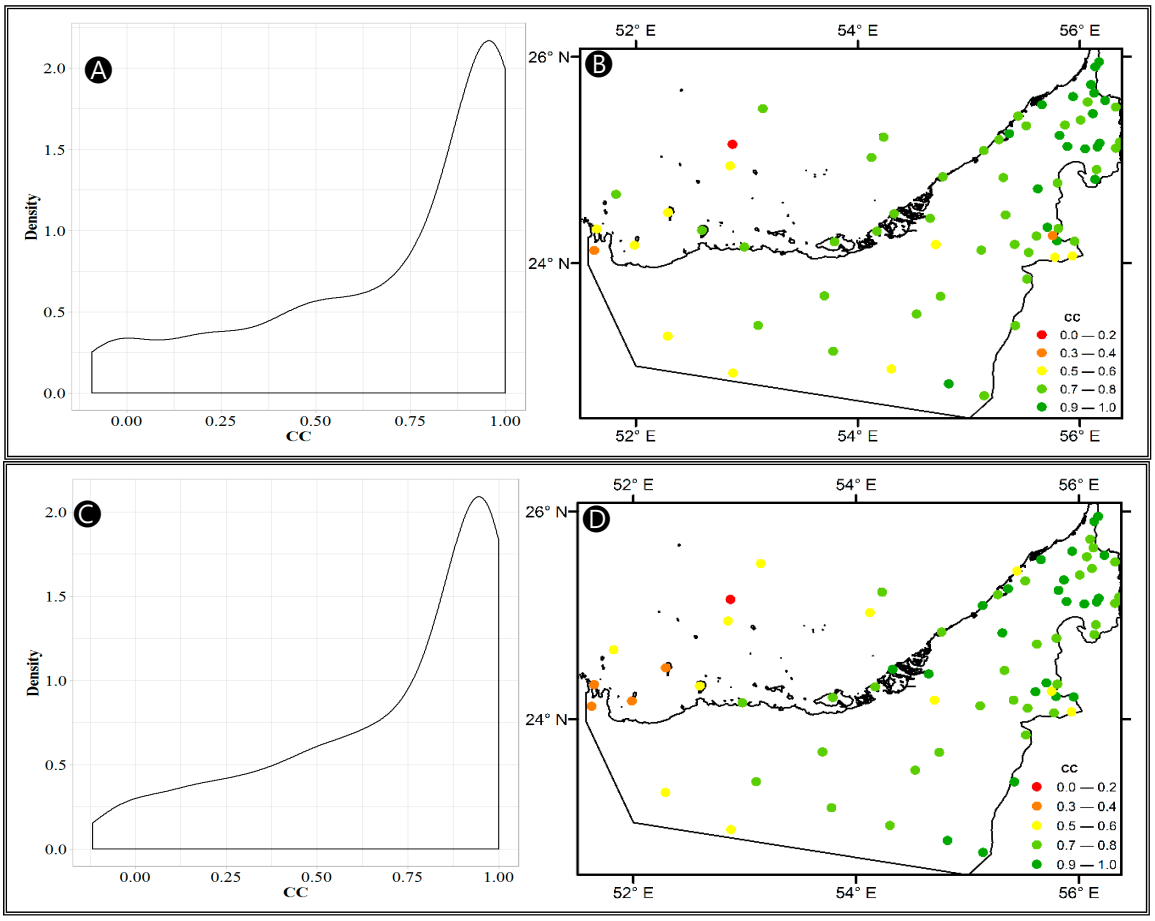

Figure 7. Spatial distribution (**B**,**D**) and Gaussian kernel density plot (**A**,**C**) of the Pearson correlation coefficient (CC) for the CMORPH (**A**,**B**) and IMERG-V06 (**C**,**D**) product.

Even though the IMERG estimate has a higher POD and better correlation with rain gauge observations, it is exceeded by the CMORPH in terms of bias and lower FAR. Overall, both products operate well in the eastern part of the UAE, which enjoys a higher annual rainfall and denser gauge distribution, as compared with those of the rest of the country. Because gauges are known to miss light precipitation [63], especially in dry regions, it seems that the performance of the IMERG is better, as its FAR and bias values are mostly due to overestimation/over-detection of light rainfall. Over the Al Hajar Mountains, both products demonstrate higher spatial variability for most of the statistical measures. This suggests that the topographic variability influences the performance of the remotely sensed precipitation products.

4.3. Event-Based Evaluation

The seven major events (Jan-2015, Dec-2015, Jan-2016, Mar-2016, Feb-2017, Mar-2017, and Nov-2018) selected for this analysis occurred in the last four years; all rain gauges were operational. An event-based analysis was conducted by calculating the statistical performance measures for each of the seven events, which was carried out to identify temporal and spatial patterns of the relationship between the rain gauge measurements and satellite-based precipitation products for all events. The spatial distribution of the total accumulated rainfall for the seven events as estimated by the CMORPH and IMERG is shown in Figure 8. The majority of these events covered only small regions of the country. The March 2017 and March 2018 events caused widespread flooding and some fatalities. Table 3 and the boxplots in Figure 9 provide summary statistics of the rainfall amounts estimated by the rain gauges for the seven storm events, together with scatter plots showing comparisons between the two satellites estimates and rain gauge observations.

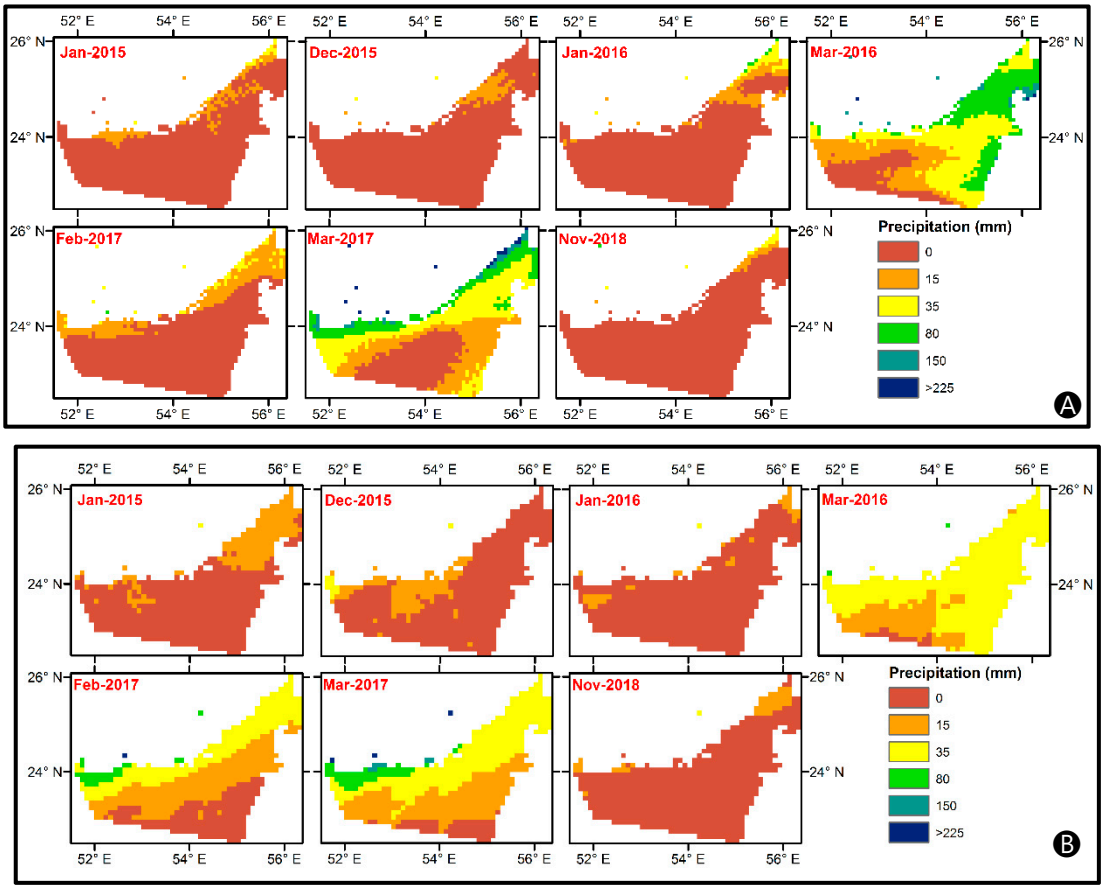

Figure 8. Spatial distribution of the seven storm events, as estimated by the CMORPH (**A**) and IMERG-V06 (**B**) products.

Table 3. Descriptive statistics of the storm events (rainfall in mm/day).

Event	Number of Rainy Records	Mean	Standard Error	Median	Standard Deviation	Range	Interquartile Range	Maximum	Skewness	Kurtosis
Jan-2015	100	9.38	1.13	4.30	11.29	47.39	10.65	47.40	1.66	2.06
Dec-2015	53	3.34	0.95	2.00	6.89	49.80	3.20	49.80	6.14	41.56
Jan-2016	140	4.18	0.52	1.90	6.09	39.59	4.25	39.60	3.08	12.03
Mar-2016	324	9.87	1.35	1.90	24.24	287.59	6.85	287.60	6.44	59.92
Feb-2017	336	3.93	0.33	1.40	6.09	33.99	4.20	34.00	2.56	6.95
Mar-2017	312	10.03	0.75	4.80	13.33	84.19	13.30	84.20	2.17	5.54
Nov-2018	88	9.04	1.39	3.70	13.04	60.59	11.65	60.60	2.21	4.73

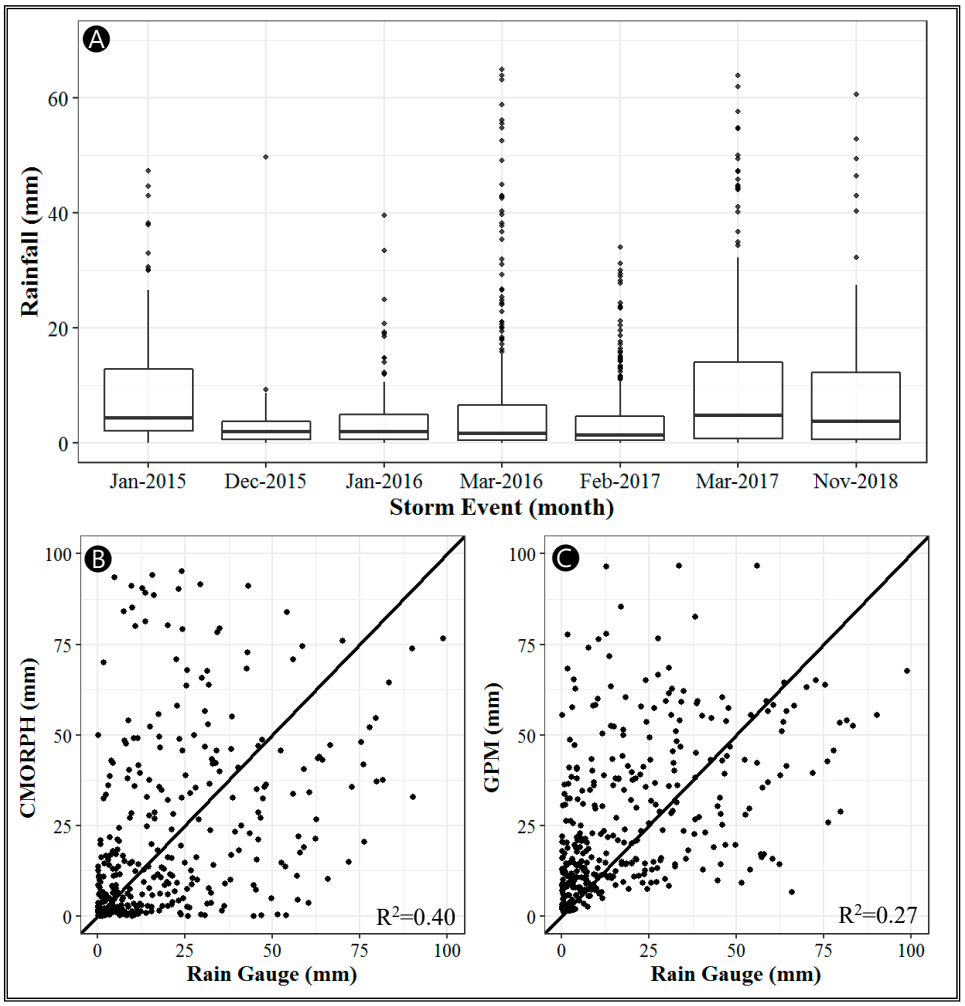

Figure 9. (**A**) Boxplots showing the distribution of the amount of rainfall recorded by the 71 gauges for the seven recent major storm events; (**B**) Scatter plot of the CMORPH and Rain Gauge; (**C**) Scatter plot of the Global Precipitation Mission (GPM) and Rain Gauge.

4.3.1. Rainfall Detection Contingency Measures

The excellent rainfall detection by the IMERG is reflected in the POD boxplots shown in Figure 10. The IMERG outperforms the CMORPH for all events. For the events Jan-2016, Feb-2017, and Mar-2017, the IMERG POD is nearly perfect (Figure 10B). The November 2018 event reported the worst POD for both products, with an interquartile range of one. The performance is reversed regarding the CSI, with the CMORPH surpassing IMERG for all events, which likely occurs because CSI accounts for false negatives. The smallest event (December 2015) corresponds to the highest CSI for the CMORPH, with IMERG showing much lower values. Both products perform poorly in terms of FAR; the median is higher than 0.50 for most of the events, as can be seen in Figure 10E,F. This finding is consistent with most studies conducted on analyzing the performance of satellite-based precipitation products [23,24]. The CMORPH performs better than the IMERG for all events, but shows higher variability. The lowest and therefore best FAR for both satellite products occurred for the January 2016 event, having both the lowest mean and median.

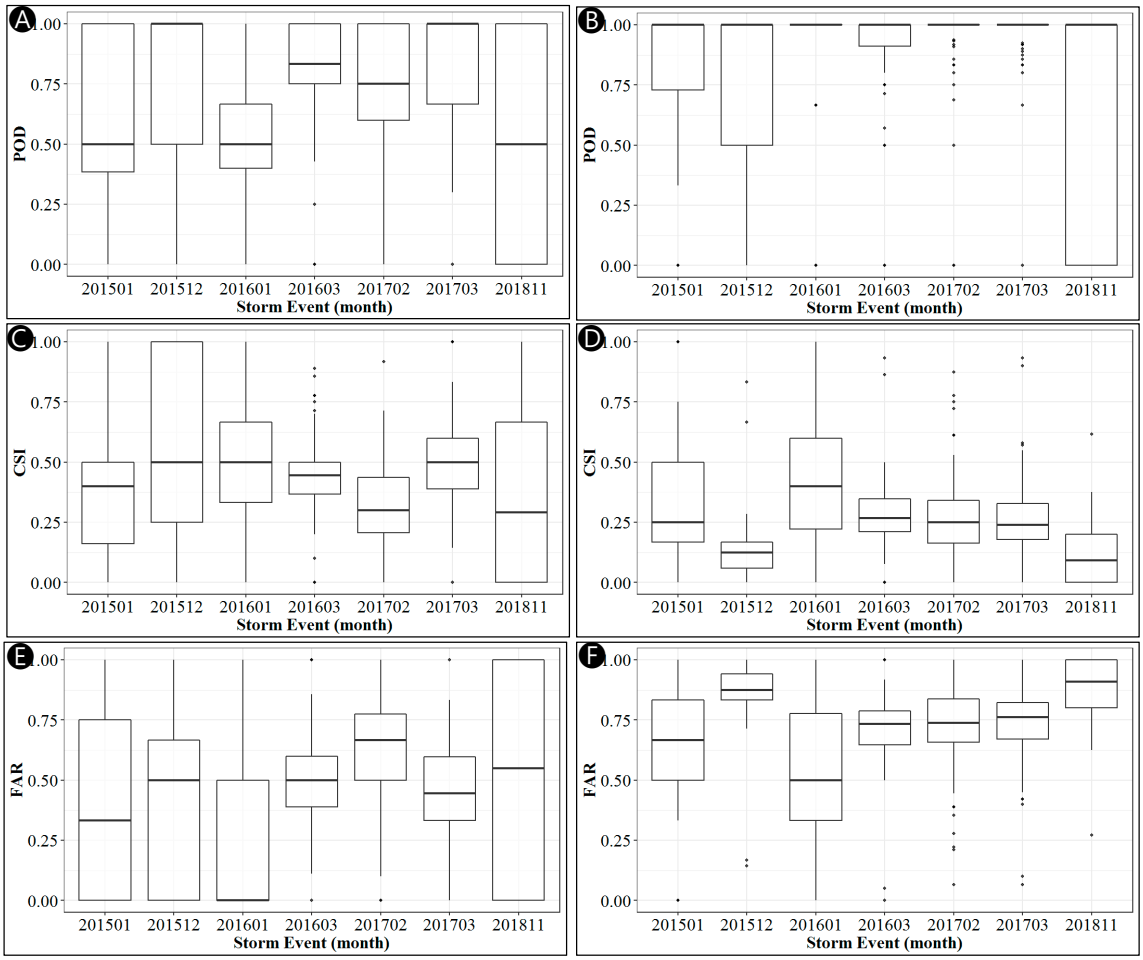

Figure 10. Boxplots showing the event-based distribution of the probability of detection (POD) (**A**,**B**), critical success index (CSI) (**C**,**D**), and false alarm ratio (FAR) (**E**,**F**) performance measures for CMORPH (**A**,**C**,**E**) and IMERG-V06 (**B**,**D**,**F**)-x-axis is labelled in YYYYMM format.

4.3.2. Bias and Error Measures

The RMSE patterns of the two products are similar for the seven events, as shown in Figure 11. The lowest RMSE error is computed for the December 2015 event. The CMORPH RBIAS showed a negative median for three out of the seven events, i.e., underestimation. However, the IMERG did not have a negative RBIAS median for all events. The CMORPH achieved smaller RBIAS values (close to zero) for all events, when compared with the IMERG. The March 2017 event has the smallest average RBIAS. However, the November 2018 event shows the most consistency, i.e., a narrower range. The IMERG overestimated rainfall for four out of the seven events with >15% average RBIAS. As is true for most of the statistics, the RBIAS also reveals that both of the products overestimated rainfall for most of the events. This is in agreement with the findings of many other researchers who demonstrated that satellite-based products overestimate low to average storm events but underestimate large events [5,19,23,26].

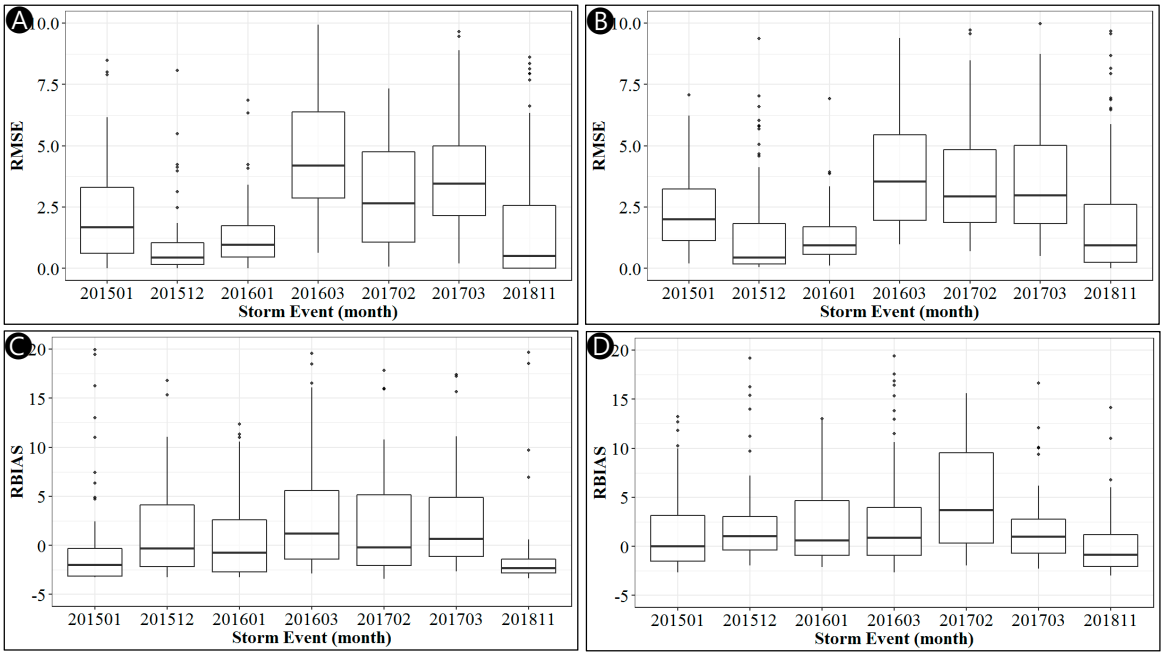

Figure 11. Boxplots showing the event-based distribution of the RMSE (**A**,**B**) and RBIAS (**C**,**D**) performance measures for CMORPH (**A**,**C**) and IMERG-V06 (**B**,**D**)-x-axis is labelled in YYYYMM format.

4.3.3. Rainfall Correlation

The CCs for all events are high, with the larger rainfall events showing the highest variability for both products (Figure 12). The December 2015 event (smallest event) presents a very strong correlation with an average of 0.89 and median of 0.98 for the IMERG product, whereas the CMORPH has an average CC of 0.94 and a median of 0.99. The lowest correlation is computed for the February 2017 event, with an average Pearson CC of 0.36 and 0.35 for IMERG and CMORPH, respectively. Overall, the IMERG has slightly higher CCs with somewhat lower variability, but the pattern is generally similar. Both products result in an average CC higher than 0.60 for all events, except for the February 2017 event.

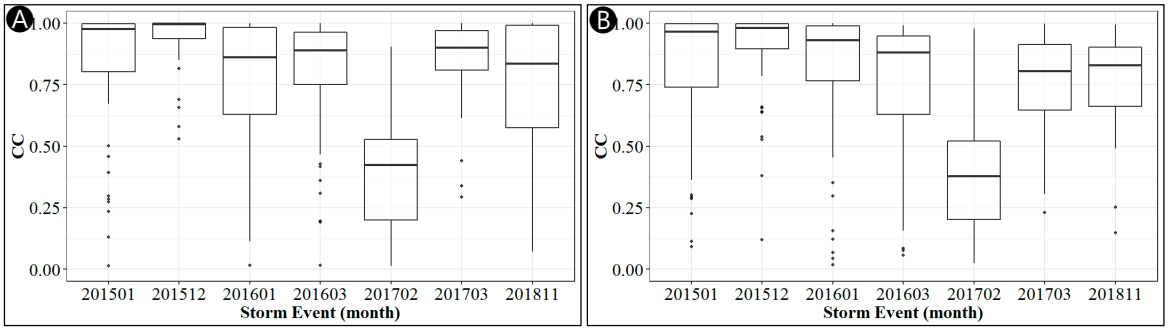

Figure 12. Boxplots showing the event-based distribution of the Pearson correlation coefficient (CC) for CMORPH (**A**) and IMERG-V06 (**B**)-x-axis is labelled in YYYYMM format.

5. Summary and Conclusions

This study investigated the performance of two high-resolution global satellite precipitation products, the CMORPH and the latest version (V06) of the GPM IMERG algorithm, over a very arid country for the 2010–2018 period. The performance was assessed using observations collected by 71 in situ rain gauge stations distributed across the country. Several commonly used quantitative,

categorical, and graphical statistical measures were used to evaluate the accuracy of these satellite-based rainfall products.

At the annual time scale, both satellite-based products followed the trends of the rain gauge observations very closely, with the IMERG-V06 overestimating rainfall and the CMORPH underestimating for most years. The IMERG-V06 exhibited higher systematic bias for small daily rainfall values and lower bias for large values than the CMORPH. These observations also applied to the random errors of the satellite-based products, as demonstrated by the CRMSE values. The underestimation of high intense rainfall by satellite-based products was reported in many previous studies [63,64]. The IMERG-V06 performed better than the CMORPH for intense rainfall (less underestimation) and much better than earlier versions of the IMERG, the results of which have been reported in previous studies. This can be attributed to the significantly higher rainfall intensity threshold adopted in V06. The two satellite products closely followed the distribution of the rainfall occurrence observed by the rain gauges, with the IMERG-V06 performing slightly better than the CMORPH.

The spatial evaluation of rainfall fields indicates that the IMERG-V06 is significantly better than the CMORPH in detecting rainfall observed by the gauge network. The average POD over the UAE by the former was 0.83, with a median of about 1.0, whereas the average was 0.69 with a median of 0.80 for the latter. However, both products recorded numerous very light rainfall events that were not detected by the rain gauges, due to sub-cloud evaporation amplified by the aridity of the region and the high temperatures (e.g., [52]), thus resulting in high FAR values. The station-based error maps agreed with the RME and CRMSE results. High systematic and random errors are attributed largely to the overestimation of light rain. In general, the performance of the CMORPH for all error measures was better than that of the IMERG-V06 across the study area. All error measures tended to be higher in the dry part of the country. Again, this was largely due to the overestimation of light rainfall. Both products achieved high Pearson CCs, especially the IMERG-V06, with an average coefficient of 0.70 and a median of 0.83, thus suggesting that the satellite rainfall estimates could be significantly improved by removing this bias.

On the basis of the performance described in this study and the well-known shortcomings of rain gauge measurements, the two reviewed products (IMERG-V06 and CMORPH) have great potential for filling spatial gaps in rainfall observations, in addition to improving the temporal resolution. The relatively high spatial and temporal resolutions can be helpful in many hydrologic and water resources applications, making them useful in the UAE and other regions with limited coverage by rain gauge networks. However, the consistent underestimation of large events by these satellite-based products will limit their applicability in flood warning and forecasting. Relaxing the precipitation threshold seems to reduce the underestimation of the IMERG product, but further improvement may be needed.

Author Contributions: T.S.A. and K.H. guided this research and contributed significantly to preparing the manuscript for publication. T.S.A., K.H., and H.O.S. developed the research methodology D.T.G. downloaded and processed the remote sensing products. D.T.G. developed the scripts used in the analysis. D.T.G. and H.O.S. performed the statistical analysis. T.S.A., K.H., H.O.S., and D.T.G. prepared the first draft. T.S.A., K.H., and H.O.S. performed the final overall proofreading of the manuscript. All authors have read and agreed to the published version of the manuscript.

Funding: This research was funded by the United Arab Emirate University Program for Advanced Research UPAR (Project No. G00002897).

Acknowledgments: The United Arab Emirates University-Research Affairs and The National Water Center at the United Arab Emirates University is gratefully acknowledged for their support. We would also like to acknowledge the National Center of Meteorology, which provided us with the in situ measurements. Gratitude is also extended to Marwan Elmubarak and Shehab Majud for following up with editing.

Conflicts of Interest: The authors declare no conflict of interest. The funders had no role in the design of the study; in the collection, analyses, or interpretation of data; in the writing of the manuscript, or in the decision to publish the results.

Appendix A

Station-based average value of the performance measures (probability of detection (POD), false alarm rate (FAR), critical success index (CSI), mean absolute error (MAE), mean error (ME), root mean square error (RMSE), relative bias (RBIAS), and Pearson correlation coefficient (CC)) for the CMORPH product versus rain gauge stations (average of all events).

Stations	POD	FAR	CSI	RMSE	MAE	ME	RBIAS	CC	Number of Observations (n)	Total Precipitation
Abu Al Abyad	0.79	0.39	0.55	3.70	0.93	−0.59	−1.81	0.71	213	269.60
Abu Al Bukhoosh	0.54	0.76	0.23	8.98	2.91	2.78	29.52	0.66	213	89.80
Abu Dhabi	0.66	0.16	0.56	2.58	0.81	0.73	3.91	0.73	213	102.80
Al Ain	0.91	0.10	0.84	0.57	0.16	0.00	−0.81	0.90	213	144.00
Al Aryam	0.70	0.52	0.44	2.66	0.82	0.53	4.14	0.65	213	116.60
Al Dhaid	0.84	0.35	0.60	1.61	0.47	0.14	6.77	0.89	213	107.40
Al Ejeili Tuwa	0.83	0.51	0.46	6.03	2.03	1.87	21.20	0.75	213	129.60
Al FarFar	1.00	0.00	1.00	2.35	0.43	−0.43	−3.11	1.00	30	13.80
Al Heben	0.61	0.25	0.49	1.97	0.67	−0.06	−1.13	0.84	89	72.20
Al Jazeera	0.59	0.34	0.44	0.98	0.31	−0.16	−1.28	0.53	213	81.20
Al Malaiha	0.57	0.51	0.35	4.06	1.01	−0.30	−0.68	0.81	213	198.20
Al Qatara	0.46	0.78	0.21	1.49	0.42	−0.07	−1.20	0.36	213	94.20
Al Qor	0.83	0.39	0.51	1.29	0.41	0.15	2.40	0.80	182	96.30
Al Shiweb	0.70	0.49	0.42	8.47	1.77	−1.49	4.14	0.76	213	476.00
Al Tawiyen	0.42	0.29	0.35	1.87	0.62	0.20	0.86	0.68	213	111.00
Alarad	0.59	0.43	0.47	2.31	0.53	−0.36	3.44	0.70	213	155.80
Alfoah	0.64	0.26	0.48	3.91	0.93	−0.84	−2.65	0.78	213	275.40
Algheweifat	0.71	0.77	0.23	1.90	0.72	0.32	4.64	0.36	213	102.80
Alkhazna	0.70	0.40	0.47	3.99	0.93	−0.87	−2.38	0.80	213	252.80
Alqlaa	0.86	0.57	0.43	2.01	0.68	0.57	9.35	0.62	213	89.40
Alquaa	0.67	0.52	0.34	0.80	0.25	0.14	0.40	0.76	213	50.90
Alwathbah	0.54	0.77	0.22	1.76	0.46	−0.03	18.41	0.58	213	82.00
Ajman	0.67	0.53	0.40	4.63	1.48	1.18	9.89	0.62	213	90.10
Bu Humrah	0.74	0.41	0.52	2.67	0.59	−0.44	−2.61	0.74	213	127.60
Burj Khalifah	0.91	0.50	0.48	3.28	1.02	0.68	4.96	0.73	151	80.80
Dalma	0.90	0.60	0.37	4.56	1.39	1.30	15.99	0.54	212	106.40
Damsa	0.49	0.33	0.27	3.52	0.81	−0.75	−2.27	0.67	213	214.00
DAS	0.14	0.98	0.02	4.43	1.75	1.75	66.00	0.21	189	4.80
Dibba Fujairah	0.25	0.00	0.25	2.50	0.58	−0.58	−2.87	0.99	30	20.10
Dhudna	0.49	0.44	0.38	2.95	0.85	0.16	−0.21	0.71	213	169.20
Falaj Al Moalla	0.76	0.33	0.53	3.34	1.01	−0.50	−0.57	0.76	213	260.20
Fujairah Port	0.81	0.32	0.52	2.13	0.66	0.31	2.04	0.79	182	113.40
Gasyoura	0.55	0.49	0.42	1.04	0.26	0.12	18.21	0.81	213	29.20
Hamim	0.76	0.31	0.47	0.77	0.22	0.07	1.84	0.45	213	23.00
Hatta	0.76	0.39	0.50	2.12	0.58	−0.32	−1.86	0.87	213	248.60
Jabal Hafeet	0.82	0.19	0.69	1.46	0.37	−0.26	−2.00	0.53	213	114.70
Jabal Jais	0.74	0.17	0.59	4.54	1.60	−1.10	−1.17	0.86	213	475.40
Jabal Mebreh	0.78	0.14	0.71	3.75	1.21	−0.89	5.90	0.84	213	366.30
Jabal Yanas	0.86	0.22	0.67	2.37	0.72	−0.13	0.01	0.84	182	208.00
Jumeirah	1.00	0.00	1.00	3.57	1.01	−0.75	−1.84	0.70	30	40.40
Khatam Al Shaklah	0.58	0.31	0.32	4.13	0.99	−0.93	−2.72	0.69	213	278.40
Madinat Zayed	0.71	0.60	0.34	2.66	0.63	−0.52	−1.81	0.76	213	143.80
Makassib	1.00	0.71	0.29	5.45	1.67	1.65	59.94	0.71	213	68.00
Manama	0.77	0.51	0.45	2.44	0.71	0.53	26.13	0.65	213	61.40
Masafi	0.74	0.41	0.53	2.75	0.83	−0.32	0.20	0.86	213	212.20
Mezaira	0.79	0.42	0.47	1.04	0.23	−0.05	1.79	0.75	213	34.40
Mukhariz	0.64	0.46	0.32	0.48	0.11	−0.03	3.44	0.53	213	20.10
Owtaid	0.57	0.43	0.34	0.98	0.23	−0.13	−0.45	0.62	213	51.10
Qarnen	0.88	0.55	0.42	8.55	2.60	2.52	30.11	0.60	213	120.10
Raknah	0.72	0.19	0.62	2.20	0.49	−0.34	−1.61	0.83	213	161.20
Ras Ganadah	0.53	0.54	0.39	4.93	1.55	1.00	167.59	0.70	213	116.30
Ras Musherib	0.79	0.73	0.26	3.14	1.12	1.02	33.82	0.55	213	70.00
Rezeen	0.63	0.33	0.53	1.60	0.40	−0.31	−2.01	0.70	213	105.60
Rowdah	0.72	0.28	0.56	3.50	0.87	−0.80	−2.63	0.60	213	225.80
Saih Al Salem	0.73	0.69	0.29	3.15	0.86	−0.09	30.10	0.68	213	172.60
Shoukah	0.76	0.46	0.40	2.57	0.67	−0.08	0.00	0.84	213	156.80
Sir Bani Yas	0.76	0.57	0.41	4.38	1.57	1.45	10.82	0.67	213	111.80

Sir Bu Nair	0.79	0.59	0.39	7.02	2.20	2.07	10.81	0.73	213	142.20
Swiehan	0.55	0.54	0.36	5.54	1.19	−1.15	−2.75	0.65	213	323.40
Um Azimul	0.47	0.33	0.31	1.56	0.38	−0.17	1.17	0.77	213	97.00
Um Ghafa	0.44	0.52	0.28	0.93	0.28	0.11	5.37	0.42	213	49.80
Umm Al Quwain	0.95	0.34	0.65	3.93	1.15	0.44	2.73	0.84	208	209.70
Wadi shahah	1.00	0.33	0.67	8.62	1.76	−1.37	−2.19	0.89	30	62.40
Yasat	0.67	0.75	0.24	2.88	1.09	0.91	17.70	0.50	213	120.20
Al Faqa	0.48	0.60	0.29	5.97	1.31	−1.01	−2.08	0.85	213	357.20
Abu D. Intl Airport	0.66	0.54	0.43	1.04	0.32	0.18	2.62	0.76	213	92.45
Al Ain Int l Airport	0.80	0.19	0.68	1.41	0.36	−0.23	−1.87	0.79	213	123.46
Dubai Int l Airport	0.66	0.15	0.52	3.53	1.03	0.75	14.78	0.89	213	124.01
Fujairah Int l Airport	0.58	0.32	0.40	1.91	0.58	0.39	3.45	0.71	213	110.16
Ras Al K. Int l Airport	0.83	0.21	0.63	2.52	0.75	−0.18	−0.08	0.86	213	221.15
Sharjah Int l Airport	0.72	0.30	0.51	3.62	1.10	0.09	6.13	0.73	213	196.46

Appendix B

Station-based average value of the performance measures (probability of detection (POD), false alarm rate (FAR), critical success index (CSI), mean absolute error (MAE), mean error (ME), root mean square error (RMSE), relative bias (RBIAS), and Pearson correlation coefficient (CC)) for the GPM product (IMERG-V06) versus rain gauge stations (average of all events).

Stations	POD	FAR	CSI	RMSE	MAE	ME	RBIAS	CC	Number of Observations (n)	Total Precipitation
Abu Al Abyad	0.83	0.83	0.17	5.38	2.00	0.88	3.53	0.65	213	269.60
Abu Al Bukhoosh	0.57	0.89	0.11	13.53	4.12	3.77	39.78	0.46	213	89.80
Abu Dhabi	0.88	0.20	0.72	1.75	0.63	0.34	1.39	0.90	213	102.80
Al Ain	0.87	0.15	0.79	0.62	0.23	−0.03	1.76	0.92	213	144.00
Al Aryam	0.93	0.80	0.20	3.46	1.23	0.85	12.74	0.79	213	116.60
Al Dhaid	0.92	0.74	0.26	1.78	0.63	0.34	4.72	0.82	213	107.40
AL Ejeili Tuwa	0.88	0.76	0.24	8.40	2.74	2.46	34.66	0.57	213	129.60
Al FarFar	1.00	0.89	0.11	1.76	0.51	−0.09	−0.68	0.83	30	13.80
Al Heben	1.00	0.63	0.37	1.33	0.57	0.23	1.24	0.85	89	72.20
Al Jazeera	0.69	0.77	0.23	1.37	0.51	0.07	17.12	0.45	213	81.20
Al Malaiha	0.76	0.70	0.29	2.61	0.85	−0.12	0.12	0.86	213	198.20
Al Qatara	0.57	0.80	0.20	1.94	0.61	0.15	5.03	0.52	213	94.20
Al Qor	0.97	0.70	0.30	1.87	0.59	0.14	7.39	0.70	182	96.30
Al Shiweb	0.86	0.73	0.27	9.32	2.08	−1.44	17.51	0.72	213	476.00
Al Tawiyen	0.72	0.66	0.32	2.28	0.80	0.44	3.58	0.66	213	111.00
Alarad	0.71	0.72	0.28	2.31	0.57	−0.23	44.09	0.74	213	155.80
Alfoah	0.86	0.70	0.30	3.97	1.11	−0.65	5.66	0.67	213	275.40
Alghewaifat	1.00	0.83	0.17	3.91	1.60	1.03	32.87	0.29	213	102.80
Alkhazna	0.81	0.78	0.21	3.52	1.01	−0.47	0.79	0.78	213	252.80
Alqlaa	1.00	0.85	0.15	3.67	1.35	1.25	81.34	0.62	213	89.40
Alquaa	0.52	0.81	0.16	0.77	0.29	0.22	4.10	0.88	213	50.90
Alwathbah	0.57	0.88	0.11	2.66	0.85	0.42	52.39	0.58	213	82.00
Ajman	0.80	0.73	0.26	2.46	0.96	0.57	5.49	0.59	213	90.10
Bu Humrah	0.67	0.75	0.22	2.94	0.77	−0.06	−0.19	0.71	213	127.60
Burj Khalifah	1.00	0.74	0.26	2.70	1.01	0.71	6.41	0.75	151	80.80
Dalma	1.00	0.83	0.17	8.90	3.70	3.36	29.07	0.38	212	106.40
Damsa	0.81	0.76	0.23	2.99	0.82	−0.37	6.17	0.74	213	214.00
DAS	0.14	0.99	0.01	7.04	2.64	2.64	83.98	0.02	189	4.80
Dibba Fujairah	1.00	0.69	0.31	1.92	0.60	−0.18	−0.88	0.84	30	20.10
Dhudna	0.61	0.75	0.24	2.93	0.92	0.16	0.59	0.60	213	169.20
Falaj Al Moalla	0.91	0.61	0.37	3.03	0.98	−0.36	−0.71	0.81	213	260.20
Fujairah Port	1.00	0.70	0.30	1.57	0.60	0.26	3.08	0.78	182	113.40
Gasyoura	0.57	0.70	0.30	1.14	0.33	0.26	16.19	0.90	213	29.20
Hamim	0.71	0.68	0.32	0.98	0.29	0.18	7.08	0.70	213	23.00
Hatta	1.00	0.69	0.31	3.28	0.88	−0.40	−0.68	0.74	213	248.60

Jabal Hafeet	0.68	0.73	0.27	1.67	0.49	0.02	0.43	0.67	213	114.70
Jabal Jais	0.91	0.73	0.26	4.97	1.80	−1.08	−0.91	0.80	213	475.40
Jabal Mebreh	0.99	0.67	0.33	4.34	1.53	−0.72	14.18	0.78	213	366.30
Jabal Yanas	1.00	0.75	0.25	2.89	1.10	0.00	0.76	0.73	182	208.00
Jumeirah	1.00	0.63	0.38	3.72	1.00	−0.92	−2.27	0.88	30	40.40
Khatam Al Shaklah	0.86	0.69	0.31	3.94	1.06	−0.70	0.78	0.86	213	278.40
Madinat Zayed	0.86	0.73	0.27	3.12	0.90	−0.06	6.60	0.69	213	143.80
Makassib	1.00	0.85	0.15	9.04	3.29	3.15	109.51	0.51	213	68.00
Manama	0.82	0.71	0.26	2.39	0.76	0.56	11.96	0.66	213	61.40
Masafi	0.83	0.77	0.23	3.25	1.05	−0.11	−0.02	0.80	213	212.20
Mezaira	0.68	0.78	0.20	1.54	0.49	0.26	13.08	0.68	213	34.40
Mukhariz	0.79	0.77	0.23	0.97	0.27	0.23	22.68	0.57	213	20.10
Owtaid	0.83	0.71	0.29	2.02	0.62	0.40	18.77	0.69	213	51.10
Qarnen	0.96	0.77	0.22	13.31	4.18	3.93	37.54	0.55	213	120.10
Raknah	0.86	0.62	0.38	2.11	0.61	−0.12	0.78	0.82	213	161.20
Ras Ganadah	0.78	0.82	0.18	4.07	1.19	0.59	180.59	0.73	213	116.30
Ras Musherib	0.97	0.83	0.17	8.20	3.08	2.89	70.55	0.32	213	70.00
Rezeen	0.81	0.71	0.27	1.53	0.45	0.02	5.71	0.75	213	105.60
Rowdah	0.86	0.69	0.31	2.79	0.79	−0.44	1.14	0.68	213	225.80
Saih Al Salem	1.00	0.74	0.26	3.06	0.88	0.10	12.06	0.80	213	172.60
Shoukah	0.96	0.62	0.38	1.51	0.54	0.06	−0.03	0.88	213	156.80
Sir Bani Yas	1.00	0.84	0.16	10.01	4.15	4.05	41.81	0.59	213	111.80
Sir Bu Nair	0.86	0.80	0.20	8.99	2.82	2.69	15.34	0.72	213	142.20
Swiehan	0.71	0.75	0.25	5.32	1.33	−0.72	−1.46	0.70	213	323.40
Um Azimul	0.71	0.63	0.37	1.40	0.41	−0.09	1.56	0.88	213	97.00
Um Ghafa	0.71	0.69	0.31	1.54	0.46	0.36	90.92	0.55	213	49.80
Umm Al Quwain	1.00	0.80	0.20	2.78	0.96	−0.09	0.87	0.80	208	209.70
Wadi shahah	1.00	0.88	0.12	9.68	1.93	−1.60	−2.57	0.94	30	62.40
Yasat	0.98	0.83	0.17	9.34	3.51	3.39	109.89	0.25	213	120.20
Al Faqa	0.69	0.72	0.28	6.16	1.49	−0.86	−1.37	0.76	213	357.20
Abu D. Intl Airport	0.81	0.71	0.28	1.95	0.72	0.53	7.97	0.80	213	92.45
Al Ain Int l Airport	0.82	0.68	0.31	1.05	0.35	0.04	2.07	0.83	213	123.46
Dubai Int l Airport	0.94	0.60	0.39	1.20	0.50	0.40	7.04	0.91	213	124.01
Fujairah Int l Airport	0.96	0.55	0.44	1.81	0.63	0.32	4.27	0.78	213	110.16
Ras Al K. Int l Airport	1.00	0.67	0.33	1.94	0.68	−0.02	0.40	0.89	213	221.15
Sharjah Int l Airport	0.99	0.60	0.40	2.57	0.88	0.05	2.84	0.80	213	196.46

References

1. Strangeways, I. *Precipitation: Theory, Measurement and Distribution*; Cambridge University Press: Cambridge, UK, 2006.
2. Bartsotas, N.; Anagnostou, E.; Nikolopoulos, E.; Kallos, G. Investigating satellite precipitation uncertainty over complex terrain. *J. Geophys. Res. Atmos.* **2018**, *123*, 5346–5359. [CrossRef]
3. Li, Z.; Yang, D.; Hong, Y. Multi-scale evaluation of high-resolution multi-sensor blended global precipitation products over the Yangtze River. *J. Hydrol.* **2013**, *500*, 157–169. [CrossRef]
4. Raich, R.; Alpert, P.; Messer, H. Vertical precipitation estimation using microwave links in conjunction with weather radar. *Environments* **2018**, *5*, 74. [CrossRef]
5. Furl, C.; Ghebreyesus, D.; Sharif, H. Assessment of the Performance of Satellite-Based Precipitation Products for Flood Events across Diverse Spatial Scales Using GSSHA Modeling System. *Geosciences* **2018**, *8*, 191. [CrossRef]
6. Sharif, H.O.; Ogden, F.L.; Krajewski, W.F.; Xue, M. Statistical analysis of radar rainfall error propagation. *J. Hydrometeorol.* **2004**, *5*, 199–212. [CrossRef]
7. Mahmoud, M.T.; Al-Zahrani, M.A.; Sharif, H.O. Assessment of global precipitation measurement satellite products over Saudi Arabia. *J. Hydrol.* **2018**, *559*, 1–12. [CrossRef]
8. Deng, L.; McCabe, M.F.; Stenchikov, G.; Evans, J.P.; Kucera, P.A. Simulation of flash-flood-producing storm events in Saudi Arabia using the weather research and forecasting model. *J. Hydrometeorol.* **2015**, *16*, 615–630. [CrossRef]
9. Gao, W.; Sui, C.H. A modeling analysis of rainfall and water cycle by the cloud-resolving WRF Model over the western North Pacific. *Adv. Atmos. Sci.* **2013**, *30*, 1695–1711. [CrossRef]
10. Xie, B.; Zhang, F. Impacts of typhoon track and island topography on the heavy rainfalls in Taiwan associated with Morakot (2009). *Mon. Weather Rev.* **2012**, *140*, 3379–3394. [CrossRef]

11. Sharif, H.O.; Al-Zahrani, M.; Hassan, A.E. Physically, Fully-Distributed Hydrologic Simulations Driven by GPM Satellite Rainfall over an Urbanizing Arid Catchment in Saudi Arabia. *Water* **2017**, *9*, 163. [CrossRef]
12. Anquetin, S.; Yates, E.; Ducrocq, V.; Samouillan, S.; Chancibault, K.; Davolio, S.; Accadia, C.; Casaioli, M.; Mariani, S.; Ficca, G.; et al. The 8 and 9 September 2002 flash flood event in France: A model intercomparison. *Nat. Hazards Earth Syst. Sci.* **2005**, *5*, 741–754. [CrossRef]
13. Germann, U.; Galli, G.; Boscacci, M.; Bolliger, M. Radar precipitation measurement in a mountainous region. *Q. J. R. Meteorol. Soc.* **2006**, *132*, 1669–1692. [CrossRef]
14. Germann, U.; Zawadzki, I. Scale dependence of the predictability of precipitation from continental radar images. Part II: Probability forecasts. *J. Appl. Meteorol.* **2004**, *43*, 74–89. [CrossRef]
15. Maddox, R.A.; Zhang, J.; Gourley, J.J.; Howard, K.W. Weather radar coverage over the contiguous United States. *Weather Forecast.* **2002**, *17*, 927–934. [CrossRef]
16. Nicholson, S.E.; Some, B.; McCollum, J.; Nelkin, E.; Klotter, D.; Berte, Y.; Diallo, B.M.; Gaye, I.; Kpabeba, G.; Ndiaye, O.; et al. Validation of TRMM and other rainfall estimates with a high-density gauge dataset for West Africa. Part II: Validation of TRMM rainfall products. *J. Appl. Meteorol.* **2003**, *42*, 1355–1368. [CrossRef]
17. McCollum, J.R.; Krajewski, W.F.; Ferraro, R.R.; Ba, M.B. Evaluation of biases of satellite rainfall estimation algorithms over the continental United States. *J. Appl. Meteorol.* **2002**, *41*, 1065–1080. [CrossRef]
18. Ebert, E.E.; Janowiak, J.E.; Kidd, C. Comparison of near-real-time precipitation estimates from satellite observations and numerical models. *Bull. Am. Meteorol. Soc.* **2007**, *88*, 47–64. [CrossRef]
19. Sapiano, M.; Arkin, P. An intercomparison and validation of high-resolution satellite precipitation estimates with 3-hourly gauge data. *J. Hydrometeorol.* **2009**, *10*, 149–166. [CrossRef]
20. Hirpa, F.A.; Gebremichael, M.; Hopson, T. Evaluation of High-Resolution Satellite Precipitation Products over Very Complex Terrain in Ethiopia. *J. Appl. Meteorol. Climatol.* **2010**, *49*, 1044–1051. [CrossRef]
21. Thiemig, V.; Rojas, R.; Zambrano-Bigiarini, M.; Levizzani, V.; de Roo, A. Validation of Satellite-Based Precipitation Products over Sparsely Gauged African River Basins. *J. Hydrometeorol.* **2012**, *13*, 1760–1783. [CrossRef]
22. Mantas, V.M.; Liu, Z.; Caro, C.; Pereira, A.J.S.C. Validation of TRMM multi-satellite precipitation analysis (TMPA) products in the Peruvian Andes. *Atmos. Res.* **2015**, *163*, 132–145. [CrossRef]
23. Wehbe, Y.; Ghebreyesus, D.; Temimi, M.; Milewski, A.; Al Mandous, A. Assessment of the consistency among global precipitation products over the United Arab Emirates. *J. Hydrol. Reg. Stud.* **2017**, *12*, 122–135. [CrossRef]
24. Wehbe, Y.; Temimi, M.; Ghebreyesus, D.T.; Milewski, A.; Norouzi, H.; Ibrahim, E. Consistency of precipitation products over the Arabian Peninsula and interactions with soil moisture and water storage. *Hydrol. Sci. J.* **2018**, *63*, 408–425. [CrossRef]
25. Michaelides, S.; Levizzani, V.; Anagnostou, E.; Bauer, P.; Kasparis, T.; Lane, J.E. Precipitation: Measurement, remote sensing, climatology and modeling. *Atmos. Res.* **2009**, *94*, 512–533. [CrossRef]
26. Tang, G.; Ma, Y.; Long, D.; Zhong, L.; Hong, Y. Evaluation of GPM Day-1 IMERG and TMPA Version-7 legacy products over Mainland China at multiple spatiotemporal scales. *J. Hydrol.* **2016**, *533*, 152–167. [CrossRef]
27. Tapiador, F.J.; Turk, F.J.; Petersen, W.; Hou, A.Y.; García-Ortega, E.; Machado, L.A.T.; Angelis, C.F.; Salio, P.; Kidd, C.; Huffman, G.J.; et al. Global precipitation measurement: Methods, datasets and applications. *Atmos. Res.* **2012**, *104*, 70–97. [CrossRef]
28. Kubota, T.; Shige, S.; Hashizume, H.; Aonashi, K.; Takahashi, N.; Seto, S.; Hirose, M.; Takayabu, Y.N.; Ushio, T.; Nakagawa, K.; et al. Global precipitation map using satellite-borne microwave radiometers by the GSMaP project: Production and validation. *IEEE Trans. Geosci. Remote Sens.* **2007**, *45*, 2259–2275. [CrossRef]
29. Joyce, R.J.; Janowiak, J.E.; Arkin, P.A.; Xie, P. CMORPH: A Method that Produces Global Precipitation Estimates from Passive Microwave and Infrared Data at High Spatial and Temporal Resolution. *J. Hydrometeorol.* **2004**, *5*, 487–503. [CrossRef]
30. NASA. Global Precipitation Measurement (GPM) Mission Overview. Available online: https://pmm.nasa.gov/GPM (accessed on 6 June 2019).
31. Huffman, G.J.; Bolvin, D.T.; Braithwaite, D.; Hsu, K.; Joyce, R.; Xie, P.; Yoo, S.H. NASA global precipitation measurement (GPM) integrated multi-satellite retrievals for GPM (IMERG). In *Algorithm Theoretical Basis Document (ATBD), Version 4.5*; 2015. Available online: https://gpm.nasa.gov/sites/default/files/document_files/IMERG_ATBD_V4.5.pdf (accessed on 8 December 2019).

32. Barrett, E. Precipitation measurement by satellites: Towards community algorithms. *Adv. Space Res.* **1993**, *13*, 119–136. [CrossRef]
33. Yilmaz, K.K.; Hogue, T.S.; Hsu, K.L.; Sorooshian, S.; Gupta, H.V.; Wagener, T. Intercomparison of rain gauge, radar, and satellite-based precipitation estimates with emphasis on hydrologic forecasting. *J. Hydrometeorol.* **2005**, *6*, 497–517. [CrossRef]
34. Shen, Y.; Xiong, A.; Wang, Y.; Xie, P. Performance of high-resolution satellite precipitation products over China. *J. Geophys. Res. Atmos.* **2010**, *115*. [CrossRef]
35. Vernimmen, R.; Hooijer, A.; Aldrian, E.; van Dijk, A. Evaluation and bias correction of satellite rainfall data for drought monitoring in Indonesia. *Hydrol. Earth Syst. Sci.* **2012**, *16*, 133. [CrossRef]
36. Ghajarnia, N.; Liaghat, A.; Arasteh, P.D. Comparison and evaluation of high resolution precipitation estimation products in Urmia Basin-Iran. *Atmos. Res.* **2015**, *158–159*, 50–65. [CrossRef]
37. Duan, Z.; Liu, J.; Tuo, Y.; Chiogna, G.; Disse, M. Evaluation of eight high spatial resolution gridded precipitation products in Adige Basin (Italy) at multiple temporal and spatial scales. *Sci. Total Environ.* **2016**, *573*, 1536–1553. [CrossRef] [PubMed]
38. Tang, G.; Clark, M.P.; Papalexiou, S.M.; Ma, Z.; Hong, Y. Have satellite precipitation products improved over last two decades? A comprehensive comparison of GPM IMERG with nine satellite and reanalysis datasets. *Remote Sens. Environ.* **2020**, *240*, 111697. [CrossRef]
39. Li, N.; Tang, G.; Zhao, P.; Hong, Y.; Gou, Y.; Yang, K. Statistical assessment and hydrological utility of the latest multi-satellite precipitation analysis IMERG in Ganjiang River basin. *Atmos. Res.* **2017**, *183*, 212–223. [CrossRef]
40. Dezfuli, A.K.; Ichoku, C.M.; Huffman, G.J.; Mohr, K.I.; Selker, J.S.; van de Giesen, N.; Hochreutener, R.; Annor, F.O. Validation of IMERG precipitation in Africa. *J. Hydrometeorol.* **2017**, *18*, 2817–2825. [CrossRef]
41. Tang, S.; Li, R.; He, J.; Wang, H.; Fan, X.; Yao, S. Comparative Evaluation of the GPM IMERG Early, Late, and Final Hourly Precipitation Products Using the CMPA Data over Sichuan Basin of China. *Water* **2020**, *12*, 554. [CrossRef]
42. Anjum, M.N.; Ding, Y.; Shangguan, D.; Ahmad, I.; Ijaz, M.W.; Farid, H.U.; Yagoub, Y.E.; Zaman, M.; Adnan, M. Performance evaluation of latest integrated multi-satellite retrievals for Global Precipitation Measurement (IMERG) over the northern highlands of Pakistan. *Atmos. Res.* **2018**, *205*, 134–146. [CrossRef]
43. Wang, X.; Ding, Y.; Zhao, C.; Wang, J. Similarities and improvements of GPM IMERG upon TRMM 3B42 precipitation product under complex topographic and climatic conditions over Hexi region, Northeastern Tibetan Plateau. *Atmos. Res.* **2019**, *218*, 347–363. [CrossRef]
44. Asong, Z.; Razavi, S.; Wheater, H.; Wong, J. Evaluation of integrated multisatellite retrievals for GPM (IMERG) over southern Canada against ground precipitation observations: A preliminary assessment. *J. Hydrometeorol.* **2017**, *18*, 1033–1050. [CrossRef]
45. Foelsche, U.; Kirchengast, G.; Fuchsberger, J.; Tan, J.; Petersen, W.A. Evaluation of GPM IMERG Early, Late, and Final rainfall estimates using WegenerNet gauge data in southeastern Austria. *Hydrol. Earth Syst. Sci.* **2017**, *21*, 6559–6572.
46. Khodadoust Siuki, S.; Saghafian, B.; Moazami, S. Comprehensive evaluation of 3-hourly TRMM and half-hourly GPM-IMERG satellite precipitation products. *Int. J. Remote Sens.* **2017**, *38*, 558–571. [CrossRef]
47. Wang, Z.; Zhong, R.; Lai, C.; Chen, J. Evaluation of the GPM IMERG satellite-based precipitation products and the hydrological utility. *Atmos. Res.* **2017**, *196*, 151–163. [CrossRef]
48. Li, C.; Tang, G.; Hong, Y. Cross-evaluation of ground-based, multi-satellite and reanalysis precipitation products: Applicability of the Triple Collocation method across Mainland China. *J. Hydrol.* **2018**, *562*, 71–83. [CrossRef]
49. Zhang, C.; Chen, X.; Shao, H.; Chen, S.; Liu, T.; Chen, C.; Ding, Q.; Du, H. Evaluation and intercomparison of high-resolution satellite precipitation estimates—GPM, TRMM, and CMORPH in the Tianshan Mountain Area. *Remote Sens.* **2018**, *10*, 1543. [CrossRef]
50. Lee, J.; Lee, E.H.; Seol, K.H. Validation of Integrated MultisatellitE Retrievals for GPM (IMERG) by using gauge-based analysis products of daily precipitation over East Asia. *Theor. Appl. Climatol.* **2019**, *137*, 2497–2512. [CrossRef]
51. Adeyewa, Z.D.; Nakamura, K. Validation of TRMM radar rainfall data over major climatic regions in Africa. *J. Appl. Meteorol.* **2003**, *42*, 331–347. [CrossRef]

52. Dinku, T.; Ceccato, P.; Connor, S.J. Challenges of satellite rainfall estimation over mountainous and arid parts of east Africa. *Int. J. Remote Sens.* **2011**, *32*, 5965–5979. [CrossRef]
53. Sultana, R.; Nasrollahi, N. Evaluation of remote sensing precipitation estimates over Saudi Arabia. *J. Arid Environ.* **2018**, *151*, 90–103. [CrossRef]
54. Mahmoud, M.T.; Hamouda, M.A.; Mohamed, M.M. Spatiotemporal evaluation of the GPM satellite precipitation products over the United Arab Emirates. *Atmos. Res.* **2019**, *219*, 200–212. [CrossRef]
55. Ouarda, T.B.; Charron, C.; Kumar, K.N.; Marpu, P.R.; Ghedira, H.; Molini, A.; Khayal, I. Evolution of the rainfall regime in the United Arab Emirates. *J. Hydrol.* **2014**, *514*, 258–270. [CrossRef]
56. NCM. Climate Yearly Report 2003–2018. 2018. Available online: https://www.ncm.ae/climate-reports-yearly.html?id=26 (accessed on 5 June 2019).
57. Frenken, K. *Irrigation in the Middle East Region in Figures AQUASTAT Survey-2008*; Water Reports 34; Food and Agriculture Organization (FAO): Rome, Italy, 2009.
58. Tan, J.; Huffman, G.J.; Bolvin, D.T.; Nelkin, E.J. IMERG V06: Changes to the Morphing Algorithm. *J. Atmos.Ocean. Technol.* **2019**, *36*, 2471–2482. [CrossRef]
59. Hou, A.Y.; Kakar, R.K.; Neeck, S.; Azarbarzin, A.A.; Kummerow, C.D.; Kojima, M.; Oki, R.; Nakamura, K.; Iguchi, T. The global precipitation measurement mission. *Bull. Am. Meteorol. Soc.* **2014**, *95*, 701–722. [CrossRef]
60. Yong, B.; Ren, L.L.; Hong, Y.; Wang, J.H.; Gourley, J.J.; Jiang, S.H.; Chen, X.; Wang, W. Hydrologic evaluation of Multisatellite Precipitation Analysis standard precipitation products in basins beyond its inclined latitude band: A case study in Laohahe basin, China. *Water Resour. Res.* **2010**, *46*. [CrossRef]
61. Huffman, G.J. Estimates of root-mean-square random error for finite samples of estimated precipitation. *J. Appl. Meteorol.* **1997**, *36*, 1191–1201. [CrossRef]
62. Wilks, D.S. *Statistical Methods in the Atmospheric Sciences*; Academic Press: Cambridge, MA, USA, 2011; Volume 100.
63. Chintalapudi, S.; Sharif, H.O.; Xie, H. Sensitivity of distributed hydrologic simulations to ground and satellite based rainfall products. *Water* **2014**, *6*, 1221–1245. [CrossRef]
64. Kubota, T.; Ushio, T.; Shige, S.; Kida, S.; Kachi, M.; Okamoto, K.I. Verification of high-resolution satellite-based rainfall estimates around Japan using a gauge-calibrated ground-radar dataset. *J. Meteorol. Soc. Jpn. Ser. II* **2009**, *87*, 203–222. [CrossRef]